Asymptotic critical behaviour of quenched random-exchange Heisenberg ferromagnets

1994 J. Phys.: Condens. Matter 6 7403

(http://iopscience.iop.org/0953-8984/6/36/022)

J. Phys.: Condens. Matter 6 (1994) 7403–7435. Printed in the UK

Asymptotic critical behaviour of quenched random-exchange Heisenberg ferromagnets

S N Kaul and M Sambasiva Rao

School of Physics, University of Hyderabad, Central University Post Office, Hyderabad 500 134, Andhra Pradesh, India

Received 14 January 1994, in final form 13 April 1994

Abstract. Asymptotic and leading 'correction-to-scaling' critical exponents and critical amplitudes for zero-field specific heat, spontaneous magnetization and initial susceptibility have been accurately determined for quenched random-exchange Heisenberg ferromagnets through an elaborate analysis of highly precise electrical resistivity, bulk magnetization and AC susceptibility data taken on amorphous $Fe_xNi_{80-x}(B,Si)_{20}$ (x = 10, 13, 16 and 20) alloys in the critical region. The values of critical exponents and universal critical amplitude ratios so obtained do not depend on composition and conform very well with the corresponding estimates given by the renormalization-group calculations for quenched random site- and bond-diluted Heisenberg ferromagnets. The amplitude ratios a_{c1}^+/a_{c1}^- and $a_{\chi 1}^+/a_{\chi 1}^-$, which are characteristic of ferromagnets with quenched random disorder and for which no theoretical estimates are presently available, seem to possess universal character for they too are composition-independent. The experimental results are consistent with the concept of scaling in that the exponent equalities $\alpha^+ = \alpha^-$, $\beta+\gamma = \beta\delta$ and $\alpha+\gamma = 2(1-\beta)$ are obeyed to a high degree of accuracy and the magnetization data satisfy the scaling equation of state characteristic of second-order phase transition. The effect of the isotropic long-range dipolar interactions on the asymptotic critical behaviour is mainly felt through the enhanced value of the A^+/A^- ratio. Only a small fraction of moments actually participates in the ferromagnetic(FM)–paramagnetic(PM) phase transition for the alloys with Fe concentration x not very far from, but above, the critical concentration x_c and this fraction reduces further at a rapid rate as x_c is approached along the FM–PM phase transition line in the magnetic phase diagram.

1. Introduction

Study of critical phenomena in quenched random site-diluted (RSDH) and bond-diluted (RBDH) Heisenberg ferromagnets has been actively pursued for more than a decade now, and yet the nature of phase transitions in these systems has defied a clear understanding so far. Conflicting theoretical predictions and inconclusive experimental results seem to be at the root of this situation as elucidated below. Theoretical attempts to calculate the magnetic susceptibility critical exponent γ for RSDH and RBDH spin systems using the high-temperature series expansion method have yielded widely different functional dependences of γ on the concentration x of the magnetic impurities; as x is lowered towards the percolation threshold x_c (critical concentration at which long-range ferromagnetic order first appears), γ increases rapidly from its value ($\simeq 1.4$) in the pure or concentrated limit (i.e. $x \simeq 1$) to a value as high as 2.5 at a concentration well above x_c for RSDH system [1], whereas it stays constant at its pure value in the entire concentration range $x_c \leqslant x \leqslant 1$ for RBDH ferromagnets [2]. Similarly, the so-called 'conventional' renormalization-group (RG) calculations [3–7], based on the random-exchange Heisenberg model (REHM), which includes both quenched RSDH

0953-8984/94/367403+33$19.50

and RBDH models, assert the following: (i) The addition of short-range frozen (quenched) disorder to a pure (ordered) spin system, which undergoes a second-order phase transition at a temperature T_c (Curie point), *does not affect* the sharpness and other critical properties of the transition if the specific heat critical exponent of the pure system, α_p, is *negative* (this result is better known as the Harris criterion [8]). (ii) The critical exponents, characterizing the paramagnetic(PM)–ferromagnetic(FM) phase transition in REHM, *do not depend* on x. (iii) In the presence of a (quenched) disorder, which introduces long-range correlations in the spin system, the FM–PM transition should get 'smeared' even if $\alpha_p < 0$. These assertions contrast with the predictions of the so-called 'unconventional' RG treatment [9–11] of REHM: (i) that a pure isotropic Heisenberg fixed point is stable only in the weak-disorder limit (i.e. for $x \to 1$); (ii) a *crossover* from *pure* to *new* critical exponents, which *depend* on x, occurs at a *composition-dependent* temperature $\epsilon_{co}(x)$ $(= (T - T_c)/T_c$ at $T = T_{co}(x)$, e.g. $\epsilon_{co} \simeq 10^0$ for $x \to 1$ whereas for $x \to x_c$ (strong-disorder limit), $\epsilon_{co} > 10^2$) even for a spin system with $\alpha_p < 0$; and (iii) in the extreme-disorder limit ($x \simeq x_c$), the critical exponents assume the Fisher-renormalized tricritical exponent values (which are the same as those given by the three-dimensional (3D) spherical model, i.e. $\alpha = -1.0$, $\beta = 0.5$, $\gamma = 2.0$, $\delta = 5.0$, $\nu = 1.0$, $\eta = 0.0$) over a wide range of temperatures extending [9] from $\epsilon \simeq 10^2$ down to $\epsilon \simeq 10^{-8}$ regardless of the dimension of the order parameter and of the range and type of interaction between spins. Though the 'unconventional' RG theories, as a result of the recent modifications [12], now support the validity of the Harris criterion even for compositions very close to x_c and for temperatures $\epsilon < 10^{-6}$, they still predict *composition-dependent effective* critical exponents in the temperature range $10^{-4} \leqslant \epsilon \leqslant 10^{-1}$. Note that the 'conventional' and 'unconventional' RG theories are *conceptually* different. The former set of theories follow two main approaches and both of them yield identical results. In the first approach [3], RG is used to derive the recursion relations for the *probability distributions* for the random potentials (which characterize quenched random spin systems) and the critical properties are determined by the fixed points of these recursion relations. In the second approach [5], a *translationally invariant* 'effective' Hamiltonian $\mathcal{H}$ is obtained by averaging a spin correlation function of the dilute continuous-spin system with respect to the random variables characterizing the dilution and then RG is employed to investigate the critical behaviour of $\mathcal{H}$. By contrast, the latter set of RG theories [9–12] use an *effective* Hamiltonian that treats a quenched random system *formally* as an equilibrium system by introducing forces of constraints. Alternatively, it is assumed that the forces of constraints establish a 'fictitious thermodynamic equilibrium' and thereby transform the spin system with quenched disorder into one with annealed disorder.

Critical behaviour near the FM–PM phase transition has been experimentally investigated in the temperature range $10^{-4} \leqslant \epsilon \leqslant 10^{-1}$ in a large number of amorphous magnetic materials [13, 14] that include 3d transition metal (TM)–metalloid (M), 3d TM–4d TM and rare earth–3d TM alloys. However, a direct comparison of the experimental results with the theoretical predictions, in most cases, is rendered meaningless due to either serious flaws in the data analysis or failure in achieving the required sensitivity in a given measurement or both [13]. A compilation [15] of the best experimental values (arrived at by using the 'single power-law' analysis) reported [13, 14, 16–24] to date for the critical exponents α, β, γ and δ, which describe the singular behaviour of specific heat $C(T)$, spontaneous magnetization $M_s(T)$, initial susceptibility $\chi_0(T)$ and the magnetization versus magnetic field (M versus H) isotherm at T_c, respectively, in the case of amorphous a-$(Ni_{1-x}Fe_x)$–M and $(Fe_{1-y}TM_y)$–M (TM = Cr or Mn) alloys demonstrates the following [15]: (i) The critical exponents for the alloys with $x \to 1$ and $y \to 0$ (i.e. in the weak-disorder limit) possess values ($\alpha \simeq -0.2$, $\beta \simeq 0.4$, $\gamma \simeq 1.31$ and $\delta \simeq 4.4$) that are fairly close to, but systematically

shifted away from, those ($\alpha \simeq -0.11$, $\beta = 0.365$, $\gamma = 1.386$ and $\delta \simeq 4.8$) theoretically predicted for a 3D isotropic Heisenberg ferromagnet; the experimentally determined values (except for the exponent α) are shifted towards the mean-field values ($\alpha = 0$, $\beta = 0.5$, $\gamma = 1$ and $\delta = 3$). (ii) The values of critical exponents increasingly deviate from those of the pure system as increasing amount of disorder is introduced into the spin system either by a progressive magnetic dilution (accomplished by replacing an increasing amount of Fe by Ni, since Ni atom carries a negligibly small moment [25] in a-$(Fe_{1-x}Ni_x)$–M alloys) or by a partial substitution of Fe by Cr or Mn (resulting in a reduction in the number of Fe–Fe ferromagnetically coupled pairs and a concomitant increase in the number of Fe–Cr or Fe–Mn antiferromagnetically coupled pairs). (iii) In the limit $x \to x_c$, the sign of such deviations depends upon whether the 3d TM replacing Fe in the above-mentioned alloy series occupies a place in the periodic table to its immediate left (e.g. Cr, Mn) or right (e.g. Ni). (iv) The exponents *do not attain* the Fisher-renormalized tricritical values at $x \simeq x_c$. While the deviations from the predictions of the 3D nearest-neighbour (NN) Heisenberg model are generally attributed [13] to long-range isotropic dipolar or Ruderman–Kittel–Kasuya–Yosida (RKKY) interactions and/or isotropic Heisenberg interactions extending well beyond the NN distance [16, 26], the dependence of critical exponents on composition is taken to imply [21, 27, 28] that the 'unconventional' RG theories describe the critical behaviour of REHM systems correctly. A careful examination of the above findings (i)–(iv), however, reveals that the observed trends are *inconsistent* with the predictions of both 'conventional' and 'unconventional' RG theories.

Recently, an elaborate analysis [29, 30], which takes into account the leading 'correction-to-scaling' (CTS) terms, of highly accurate 'zero-field' susceptibility, $\chi_0(T)$, and electrical resistivity, $\rho(T)$, data taken on a-$Fe_xNi_{80-x}B_{19}Si_1$ alloys in the critical region has yielded true *asymptotic* values of the critical exponents γ and α that *do not depend on composition* and are indistinguishable (within the error limits) from the corresponding values given by the RG theory [31] for pure isotropic spin systems with space (d) as well as spin (n) dimensionality of 3 (i.e. systems with $d = n = 3$). The results of this analysis have also demonstrated that the systematic deviations in the case of the exponents γ and α observed earlier can be traced back to the customary practice of neglecting the CTS terms completely and using the 'single power-law' method to analyse the data taken over a range of temperatures that embraces the critical region. The spurious nature of the deviations suggests that the previously determined values of the exponents β and δ are not true asymptotic values, and that a reanalysis, which gives due consideration to the confluent singularity terms, of the bulk magnetization data already available [13, 14, 17, 22] on some compositions in the glassy alloy series a-$Fe_xNi_{80-x}B_{19}Si_1$ is called for. However, inclusion of the CTS terms in the data analysis demands a far greater precision in the measurements than achieved hitherto. This realization prompted us to undertake high-precision magnetization measurements on the amorphous alloys with $x = 10$, 13, and 16 in the above-mentioned series and on a-$Fe_{20}Ni_{60}B_{20}$. Moreover, we have taken *new* sets of AC ('zero-field') susceptibility, $\chi_0(T)$, data on samples (with composition $x = 10$, 13 and 16) the *same* as those used in our recent resistivity, $\rho(T)$, measurements [30] and then performed magnetization, $M(H, T)$, measurements on them with a view to test the validity of the claim recently made by Güntzel and Westerholt [28] that the low-field AC susceptibility is not well suited to study critical behaviour in metallic glasses and to investigate in depth the possible bearing of deviations from the straight-line Arrott plot isotherms observed [13, 14, 22, 24, 28] at low fields, usually encountered in amorphous ferromagnets, on the critical behaviour. The fact that all three physical quantities, i.e. $\rho(T)$, $\chi_0(T)$ and $M(H, T)$, have been measured for the *same* alloy ribbons not only permits a detailed comparison between the results of $\chi_0(T)$

and $M(H, T)$ measurements in the critical region but also gets rid of the complications arising from the variations in composition, if present, in samples from the same (different) alloy batch (batches).

2. Experimental details

Amorphous (a-) $Fe_xNi_{80-x}B_{19}Si_1$ ($x = 10, 13, 16$) and $Fe_{20}Ni_{60}B_{20}$ alloys were prepared in the form of long ribbons of cross section 0.04×2 mm^2 by the single-roller melt-quenching technique under high-purity argon (inert) atmosphere. That the ribbons so fabricated are in the amorphous state was verified by the x-ray diffraction method using Mo K_α radiation and later confirmed by the high-resolution electron microscopic technique. A detailed compositional analysis [29] was then carried out on ribbons that did not reveal any crystalline regions upon electron microscopic examination. From such an analysis and the observed composition dependence [13–15, 17, 20, 22, 25, 29, 30] of T_c, the concentration fluctuations in the samples in question are expected to give rise to fluctuations in T_c of the order $\delta T_c \simeq 0.1$ K. Our recent resistivity results [30] on a-$Fe_xNi_{80-x}B_{19}Si_1$ alloys do indeed show that the 'rounding' of the transition at T_c occurs for $|T - T_c| < 0.1$ K. Therefore, the data taken in the reduced temperature range $\leqslant \delta T_c/T_c$ have been excluded from the analysis.

Previous high-resolution (relative accuracy better than 1 ppm) electrical resistivity measurements [30] carried out on a-$Fe_xNi_{80-x}B_{19}Si_1$ ($x = 10, 13, 16$) alloy ribbons of length 60 mm using the four-probe DC method were extended to yet another composition a-$Fe_{20}Ni_{60}B_{20}$. The $\rho(T)$ data on this sample were taken at temperatures $\simeq 30$ mK apart in the region $-0.1 \leqslant \epsilon = (T - T_c)/T_c \leqslant 0.1$ keeping sample temperature constant at a given setting to within ± 10 mK by means of a proportional, integral and derivative (PID) temperature controller. Other relevant details regarding these measurements are given in our earlier paper [30]. The 60 mm long resistivity sample (ribbon piece) of a given alloy composition was cut into *three* strips, each $\simeq 20$ mm in length, which were then stacked one above the other to form the sample for AC susceptibility, $\chi_{ac}(T)$, measurements. High-precision (relative accuracy better than 10 ppm) $\chi_{ac}(T)$ data were recorded on the samples with composition $x = 10$, 13 and 16 (similar measurements on the $Fe_{20}Ni_{60}B_{20}$ sample could not be carried out because its Curie temperature lies just above the maximum temperature that the experimental set-up can presently handle) at 25 mK intervals in the temperature range $-0.05 \leqslant \epsilon \leqslant 0.05$ in a RMS AC driving field of $H_{ac} = 100$ mOe and frequency 87 Hz, using the mutual inductance method [31]. The sample temperature, monitored by a precalibrated platinum resistance sensor, as in the $\rho(T)$ case, was kept constant to within ± 10 mK during the measurement period at every fixed temperature setting by the PID temperature controller. Magnetization (M) versus magnetic field (H_{ex}) isotherms (temperature stability better than ± 40 mK) were measured at 0.15 K intervals in the critical region $-0.05 \leqslant \epsilon \leqslant 0.05$ and at temperatures 5 K apart for $\epsilon > 0.05$ by means of the PAR 4500 vibrating sample magnetometer in fields up to 10 kOe on a-$Fe_xNi_{80-x}(B,Si)_{20}$ alloys with $x = 10$, 13, 16 and 20. Each isotherm was obtained by measuring M at 25 predetermined but fixed (to within ± 1 Oe) values of H_{ex} in the range 0.1 kOe $\leqslant H_{ex} \leqslant 10$ kOe. The sample employed for $M(H_{ex}, T)$ measurements was in the form of a *pile* of *twelve* $\simeq 5$ mm long pieces cut from *three* $\simeq 20$ mm long strips (one 60 mm long strip) of composition $x = 10$ or 13 or 16 in the amorphous alloy series $Fe_xNi_{80-x}B_{19}Si_1$ ($Fe_{20}Ni_{60}B_{20}$) used earlier for $\chi_{ac}(T)$ ($\rho(T)$) measurements. The sample temperature was measured by precalibrated platinum resistance sensor and copper–constantan thermocouple for temperatures below and above

300 K, respectively. H_{ac} and H_{ex} were directed along the length of the strips within the ribbon plane in $\chi_{ac}(T)$ and $M(H_{ex}, T)$ measurements to minimize the demagnetizing effects. The demagnetizing factor for the samples used in both these measurements was determined by the low-field ($\leqslant$ 20 Oe) magnetization data and the external field, H_{ex}, was corrected for the demagnetizing field, H_{dem}, to obtain the field, $H = H_{ex} - H_{dem}$, experienced by the spins within the sample.

3. Results and data analysis

3.1. Zero-field specific heat and temperature derivative of resistivity

For concentrations close to, but higher than, the critical concentration x_c, only a small fraction of spins actually participates in the FM–PM phase transition [13, 14, 17] and this fraction decreases rapidly as $x \to x_c^+$, implying thereby that a small amount of magnetic entropy is released at T_c for such systems. As a consequence, it is impossible to detect the singularity in the magnetic part of specific heat, $C_M(T)$, at T_c for alloys with $x \simeq x_c^+$ even under the most favourable conditions. An effective way to tackle this problem is to exploit the well known relation [32], i.e. $d\rho_M(T)/dT \propto C_M(T)$, between C_M and the temperature derivative of the magnetic part of electrical resistivity for temperatures in the close proximity to T_c and study the critical behaviour of $C_M(T)$ indirectly by measuring $\rho(T)$ in the critical region. An accuracy greater by three or more orders of magnitude routinely achieved in resistivity measurements than in specific heat measurements permits detection of the anomaly at T_c with ease. That a direct correlation between $d\rho_M(T)/dT$ and $C_M(T)$ in the critical region exists in spin systems with quenched disorder has previously been experimentally demonstrated [33, 34] for several amorphous TM–M alloys including one of the alloys of present interest [34], i.e. $Fe_{20}Ni_{60}B_{20}$.

The temperature derivative of resistivity (evaluated by the three-point differentiation method) normalized to the value of resistivity at T_c $(d\rho(T)/dT)/\rho(T_c) \equiv \alpha_r$, as a function of temperature in the reduced temperature range $-0.05 \leqslant \epsilon \leqslant 0.05$ for a-$Fe_{20}Ni_{60}B_{20}$ is shown in figure 1. The previously published [30] $\alpha_r(T)$ data on the amorphous alloys with $x = 10$, 13 and 16 in the series $Fe_xNi_{80-x}B_{19}Si_1$ are also included in this figure for comparison. The data for the former sample have been analysed in the same manner as those for the latter alloys. We only briefly outline the method of analysis here since the details have already been given elsewhere [30]. Theoretical fit to the $\alpha_r(T)$ data is attempted based on the expression

$$\alpha_r = (A^{\pm}/\alpha^{\pm})(\pm\epsilon)^{-\alpha^{\pm}}[1 + a_{c1}^{\pm}\alpha^{\pm}(\pm\epsilon)^{\Delta_1} + a_{c2}^{\pm}\alpha^{\pm}(\pm\epsilon)^{\Delta_2}] - (A^{\pm}/\alpha^{\pm}) + B^{\pm} \qquad (1)$$

(where the plus and minus signs denote temperatures above and below T_c, and $A^{\pm}$ ($a_{c1}^{\pm}$, $a_{c2}^{\pm}$) and $\alpha^{\pm}(\Delta_1, \Delta_2)$ are the *asymptotic* (leading 'correction-to-scaling') critical amplitudes and critical exponents, respectively) given by the so-called 'conventional' RG theories [3–7, 15, 30, 35, 36]. These theories consider the quenched disorder in $d = n = 3$ NN isotropic spin system as an *irrelevant scaling* field and hence predict that an additional leading confluent correction term, characterized by the exponent [6, 7, 29, 35, 36] $\Delta_1 = |\alpha_p|$, should appear in (1) besides the one present in pure systems and involving the exponent Δ_2. By contrast, the so-called modified 'unconventional' RG theories [12] assert that the *effective* critical exponents $\alpha_{eff}^{\pm}$, corresponding to the case when $a_{c1}^{\pm} = a_{c2}^{\pm} = 0$ in (1), are *composition-dependent* unless T_c is approached closer than $\epsilon \simeq 10^{-6}$. In view of the above theoretical predictions, to begin with, we fit the $\alpha_r(T)$ data for $T < T_c$ and $T > T_c$ separately to

a single power law by setting $a_{c1}^{\pm} = a_{c2}^{\pm} = 0$ in (1) and use a range-of-fit analysis in which the change, if any, in the values of the fitting parameters $A^{\pm}$, $B^{\pm}$, $\alpha^{\pm}$ and $T_c^{\pm}$ is monitored as the temperature range ($\epsilon_{min} \leqslant \epsilon \leqslant \epsilon_{max}$) of the fit is narrowed down by raising (lowering) ϵ_{min} (ϵ_{max}) towards ϵ_{max} (ϵ_{min}) while keeping ϵ_{max} (ϵ_{min}) fixed at a given value. The results of this single power-law analysis (henceforth referred to as AA) for a-$Fe_{20}Ni_{60}B_{20}$ coupled with those yielded by the same analysis for other compositions ($x = 10, 13, 16$) previously [30] present the following main features. (i) $T_c^- \simeq T_c^+$ and $\alpha^- \simeq \alpha^+$ within the error limits. (ii) The exponent α stays constant in a narrow temperature interval $|\epsilon_{min}^{\pm}| \leqslant |\epsilon| \leqslant |\epsilon_{max}^{\pm}|$ only and within that interval its value $\alpha = -0.15 \pm 0.02$ is independent (within the error limits) of the Fe concentration. (iii) The ratios $A^+/A^- \simeq 1.55$ and $[B^+ - (A^+/\alpha^+)]/[B^- - (A^-/\alpha^-)] \simeq 1.6$ regardless of the Fe concentration. Failure of data to satisfy the equality $B^+ - (A^+/\alpha^+) = B^- - (A^-/\alpha^-)$ dictated by the requirement that, for $\alpha < 0$, $d\rho^+/dT = d\rho^-/dT$ at $T = T_c$, necessitates inclusion of the confluent singularity terms in the analysis. As a first step in this direction, $\alpha_r(T)$ data for $T < T_c$ and $T > T_c$ have been least-squares fitted to the expression that includes the first leading correction term only, i.e. equation (1) with $a_{c2}^{\pm} = 0$, and agreement with the experimental data is optimized by varying the parameters $A^{\pm}$, $B^{\pm}$, $\alpha^{\pm}$, $T_c^{\pm}$, $a_{c1}^{\pm}$ and Δ_1. Though these fits are superior to the 'single power-law' fits and the values of $T_c^{\pm}$ and $\alpha^{\pm}$ are reasonably accurate (e.g. $\alpha^- \simeq \alpha^+ = -0.115 \pm 0.008$), values of $A^{\pm}$, $B^{\pm}$, $a_{c1}^{\pm}$ and Δ_1 fluctuate a lot when the range of fit is altered. We therefore fit the $\alpha_r(T)$ data to (1) for $T < T_c$ and $T > T_c$ separately, using the range-of-fit analysis and a non-linear least-squares-fit computer program that treats $A^{\pm}$, $B^{\pm}$, $\alpha^{\pm}$, $a_{c1}^{\pm}$, $a_{c2}^{\pm}$ and $T_c^{\pm}$ as free fitting parameters, but keeps Δ_1 and Δ_2 fixed at a given value in the ranges $0.01 \leqslant \Delta_1 \leqslant 0.20$ and $0.35 \leqslant \Delta_2 \leqslant 0.75$. The same procedure is repeated for another fixed set of values for Δ_1 and Δ_2, which differ from the previous ones by ± 0.01. Best fits, as inferred from the least values of the sum of the deviation squares, χ^2, are obtained for $\Delta_1 = 0.11 \pm 0.05$ and $\Delta_2 = 0.55 \pm 0.08$, with the values for the remaining parameters that have an undesirably large uncertainty (e.g. typical values for the asymptotic exponent are $\alpha^+ = -0.115 \pm 0.015$ and $\alpha^- = -0.120 \pm 0.015$) but are otherwise close to those determined by the following procedure and listed in table 1. Realizing that the large uncertainty mainly stems from the correlation between different parameters in a multiparameter fit, and that the above values of Δ_1 and Δ_2 conform very well with the theoretically predicted [36–38] estimates, substantial reduction in the uncertainty is achieved by imposing the condition $T_c^- = T_c^+$ and by keeping Δ_1 and Δ_2 constant at $\Delta_1 = 0.11$ and $\Delta_2 = 0.55$. With these constraints, the range-of-fit analysis and the least-squares fitting method (the 'so-called' CTS analysis) yield the most optimal values for the parameters $T_c^{\pm}$, $\alpha^{\pm}$, $A^{\pm}$, $B^{\pm}$, $a_{c1}^{\pm}$ and $a_{c2}^{\pm}$ displayed in table 1. The theoretical fits based on these parameter values and denoted in figure 1 by the full curves can be seen to describe the observed variation of $\alpha_r(T)$ very well for $|\epsilon| \leqslant |\epsilon_{co}|$; the data points start deviating from these fits for $|\epsilon| > |\epsilon_{co}|$. This observation is made all the more obvious by the deviation plot shown in figure 2 for a-$Fe_{20}Ni_{60}B_{20}$. From figure 2, which depicts the percentage deviation of the data from the best AA or CTS fit as a function of reduced temperature, it is evident that the CTS fits closely reproduce the observed variation of α_r with T over a wide temperature range whereas the AA fits present *systematic* deviations from the actual data in the entire temperature range covered in the fits. Thus, the data presented in figure 2 highlight the importance of the CTS terms and assert that the CTS analysis provides an accurate means of determining the asymptotic and correction-to-scaling critical exponents and amplitudes as well as the crossover temperature $|\epsilon_{co}|$, which, in turn, determines the extent of the asymptotic critical region in the materials under consideration. The same inference can be

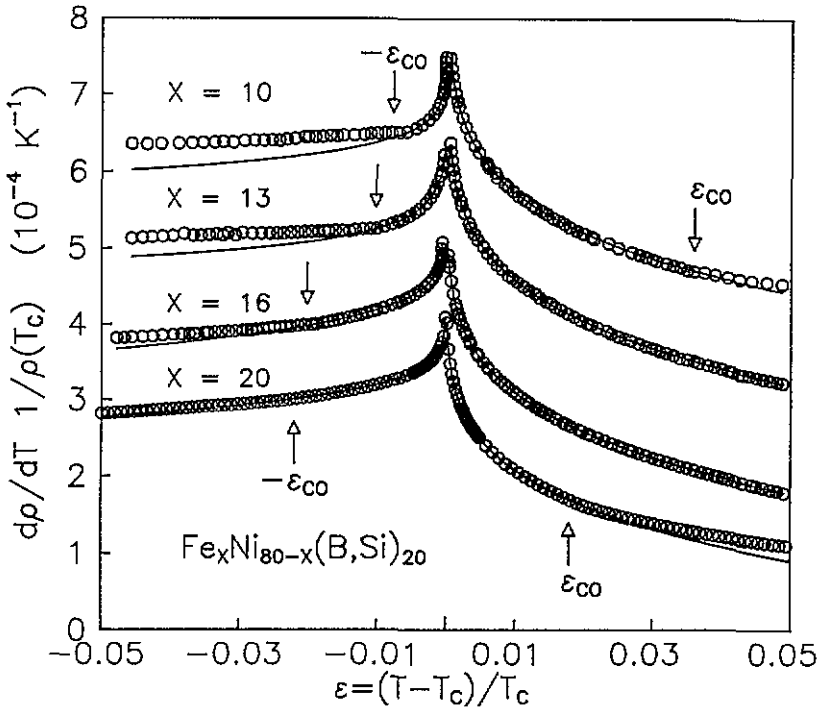

Figure 1. Normalized temperature derivative of resistivity as a function of reduced temperature for amorphous $Fe_xNi_{80-x}(B,Si)_{20}$ alloys in the range $-0.05 \leqslant \epsilon = (T - T_c)/T_c \leqslant 0.05$. The full curves through the data points are theoretical fits based on equation (1). For the sake of clarity, only one-eighth of the total number of data points are shown in this figure and the data points corresponding to temperatures in the immediate vicinity of T_c are deleted. Note that the zero on the ordinate scale should read as 1, 2 and 3, respectively, for the alloys with $x = 13$, 16 and 20.

drawn from the deviation plots for the alloys with $x = 10$, 13 and 16 shown in figure 8 of [30].

3.2. *'Zero-field' susceptibility*

The observed variation of AC susceptibility, corrected for demagnetization, i.e. $\chi_0(\epsilon) = \chi_{meas}(\epsilon)/[1 - N\chi_{meas}(\epsilon)]$ where N is the demagnetizing factor, with temperature in the critical region is depicted in figure 3. The 'conventional' RG theories [3–7, 15, 29, 35, 36] yield a temperature dependence of 'zero-field' (initial) susceptibility, $\chi_0(\epsilon)$, for temperatures ($\epsilon \geqslant 0$) not too close to T_c of the form

$$\chi_0(\epsilon) = \Gamma\epsilon^{-\gamma}(1 + a^+_{\chi 1}\epsilon^{\Delta_1} + a^+_{\chi 2}\epsilon^{\Delta_2}) \qquad \epsilon > 0 \tag{2}$$

which includes the leading 'correction-to-scaling' (CTS) confluent singularity terms. Experimentally, however, it is customary to fit $\chi_0(\epsilon)$ data taken over a fairly wide temperature range near T_c to a *single* power law

$$\chi_0(\epsilon) = \Gamma_{eff}\epsilon^{-\gamma_{eff}} \qquad \epsilon > 0 \tag{3}$$

where Γ_{eff} and γ_{eff} are the *effective* critical amplitude and critical exponent, respectively. According to the 'unconventional' RG theories [9–12], equation (3) describes the temperature

Table 1. Asymptotic and 'correction-to-scaling' specific heat critical exponents and critical amplitudes for amorphous $Fe_xNi_{80-x}(B,Si)_{20}$ alloys from the $d\rho/dT$ data. Note that the 'so-called' crossover temperatures ϵ_{co} for $T < T_c$ and $T > T_c$ are ϵ^-_{min} and ϵ^+_{max}, respectively.

Alloy composition, Fe/Ni/B/Si	$T_c^+ = T_c^-$ (K)	Range of fit ϵ^-_{min} $[\epsilon^+_{min}]$ (10^{-3})	Range of fit ϵ^-_{max} $[\epsilon^+_{max}]$ (10^{-3})	A^- $[A^+]$ $(10^{-3}\ K^{-1})$	B^- $[B^+]$ $(10^{-3}\ K^{-1})$	α^- $[\alpha^+]$	a^-_{c1} $[a^+_{c1}]$	a^-_{c2} $[a^+_{c2}]$	Δ_1 $[\Delta_2]$	χ^2 (10^{-10})
10/70/19/1	187.03(5)	−7.5 [0.50]	−0.50 [36.0]	0.075(1) [0.116(1)]	0.330(5) [0.161(2)]	−0.114(5) [−0.114(5)]	2.80(60) [0.23(5)]	−1.40(65) [−1.45(25)]	0.11(6) [0.54(10)]	0.76 1.48
13/67/19/1	268.64(6)	−10.0 [0.35]	−0.37 [45.0]	0.073(1) [0.110(1)]	0.335(5) [0.155(2)]	−0.115(5) [−0.113(5)]	2.45(65) [0.25(5)]	−2.45(65) [−2.45(25)]	0.10(5) [0.56(10)]	0.95 0.99
16/64/19/1	341.45(5)	−20.0 [0.28]	−0.29 [55.0]	0.071(1) [0.105(1)]	0.305(5) [0.130(2)]	−0.111(5) [−0.110(5)]	3.50(50) [0.38(7)]	−2.75(75) [−2.85(25)]	0.12(6) [0.55(10)]	1.11 1.13
20/60/20/0	425.56(4)	−22.0 [0.16]	−0.07 [20.0]	0.066(2) [0.101(1)]	0.295(12) [0.138(8)]	−0.114(1) [−0.114(3)]	4.12(15) [0.55(7)]	−2.62(2) [−2.66(4)]	0.11(5) [0.55(8)]	0.07 0.31

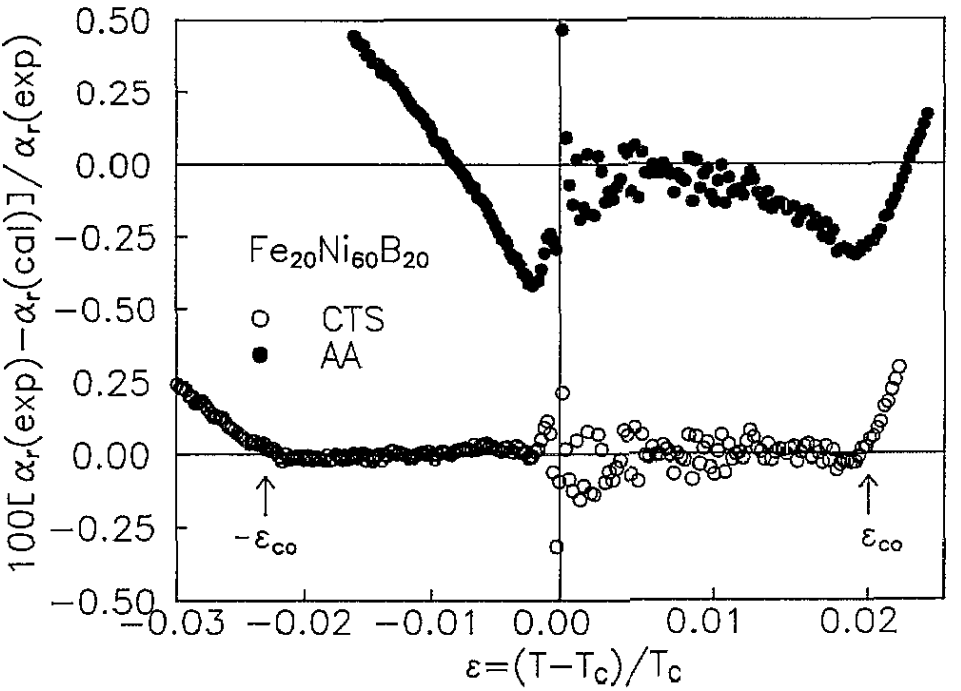

Figure 2. Percentage deviation of the $\alpha_r(T)$ data from the best AA (●), based on equation (1) with $a_{c1}^{\pm}$ and $a_{c2}^{\pm}$ set equal to zero and the choice of parameters $A^+ = 0.12 \times 10^{-3}$ K^{-1} ($A^- = 0.065 \times 10^{-3}$ K^{-1}), $B^+ = 0.103 \times 10^{-3}$ K^{-1} ($B^- = 0.42 \times 10^{-3}$ K^{-1}) and $\alpha^+ = -0.14$ ($\alpha^- = -0.18$), and CTS (○), based on equation (1) with the choice of the parameters given in table 1, least-squares fits. The arrows indicate the crossover temperature ϵ_{co}.

variation of $\chi_0(\epsilon)$ in the crossover region correctly and γ_{eff} is *composition-dependent.* Considering the relation that exists between γ_{eff} and γ for temperatures very close [29] to T_c, i.e.

$$\gamma_{eff}(\epsilon) = d[\ln \chi_0^{-1}(\epsilon)]/d(\ln \epsilon) = \gamma - a_{\chi 1}^{+}\Delta_1 \epsilon^{\Delta_1} - a_{\chi 2}^{+}\Delta_2 \epsilon^{\Delta_2} \tag{4}$$

γ_{eff} could *significantly differ* from the theoretically ('conventional' RG theories) predicted *asymptotic* (universal) critical exponent γ and it is only in the limit $\epsilon \to 0^+$ that $\gamma_{eff}(\epsilon)$ coincides with γ, i.e. $\gamma = \lim \epsilon \to 0^+[\gamma_{eff}(\epsilon)]$. The corresponding relation between Γ_{eff} and Γ is [29]

$$\Gamma_{eff}(\epsilon) = \Gamma(1 + a_{\chi 1}^{+}\epsilon^{\Delta_1} + a_{\chi 2}^{+}\epsilon^{\Delta_2})\epsilon^{-(a_{\chi 1}^{+}\Delta_1 \epsilon^{\Delta_1} + a_{\chi 2}^{+}\Delta_2 \epsilon^{\Delta_2})} = \Gamma N \tag{5}$$

where N represents the expression by which Γ is multiplied to yield the product Γ_{eff} in (5). It is evident from equations (2)–(5) that a prior knowledge of Γ_{eff}, γ_{eff} and T_c is required for extracting values of Γ, γ, $a_{\chi 1}^{+}$, $a_{\chi 2}^{+}$, Δ_1 and Δ_2 from the $\chi_0(\epsilon)$ data. High accuracy in the determination of T_c and γ_{eff} (and hence of Γ_{eff}) is achieved by a method [39] (henceforth referred to as the KF analysis) that makes use of the following alternative form of equation (3), i.e.

$$X(T) \equiv \chi_0^{-1}(T)[d\chi_0^{-1}(T)/dT]^{-1} = (T - T_c)/\gamma_{eff} = (T_c/\gamma_{eff})\epsilon. \tag{6}$$

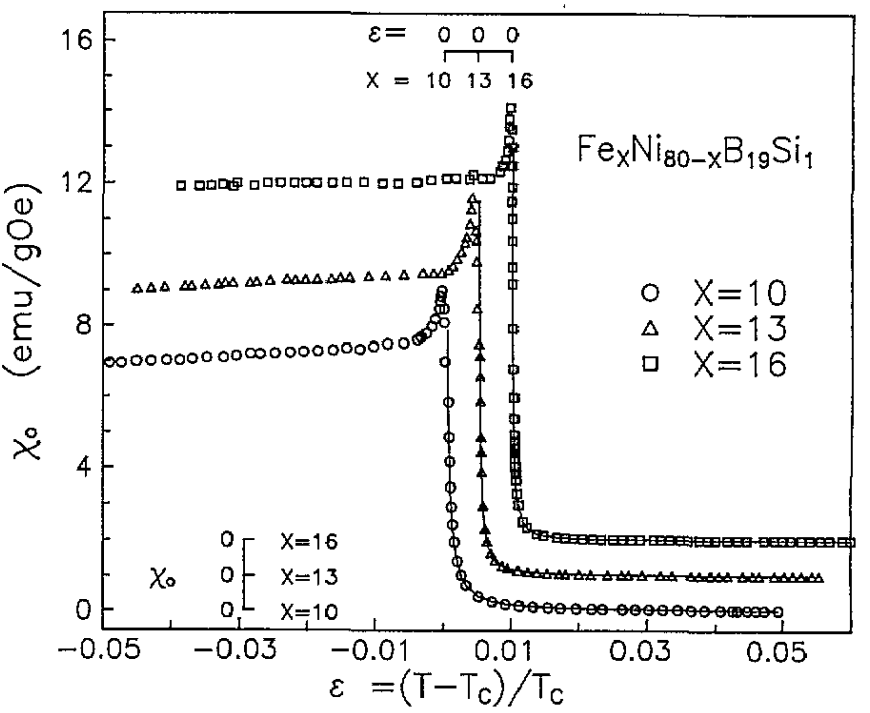

Figure 3. Variation of initial (AC) susceptibility with temperature in the range $-0.05 \leqslant \epsilon \leqslant 0.05$. Note the change of scale for the data of the alloys with $x = 10$, 13 and 16. For the sake of clarity, only one-quarter of the total number of data points are shown in this figure.

According to this method, the $X(T)$ versus T plot in the asymptotic critical region (ACR), where $\chi_0(T)$ can be approximated by a power law (equation (3)), is a straight line whose slope is $1/\gamma_{\text{eff}}$ and intercept on the T axis yields T_c (note that if the value of T_c, determined by the KF analysis, is used to construct the $X(T)$ versus ϵ plot in the ACR, the resulting plot should, again, be a straight line but now this straight line passes through the origin and possesses a slope T_c/γ_{eff}, cf equation (6)). The $X(T)$ versus ϵ plots shown in figure 4 for the amorphous alloys with $x = 10$, 13 and 16 testify to the validity of equation (6) (and hence of equation (3)) in a narrow temperature range above T_c. Data points, however, start deviating from the least-squares-fitted straight lines at a temperature ϵ_{co} (shown in figure 4 by downward arrows) and the deviations grow as ϵ is increased above ϵ_{co}. In view of the definition

$$\gamma_{\text{eff}}(\epsilon) = [\chi_0(\epsilon)\, \mathrm{d}\chi_0^{-1}(\epsilon)/\mathrm{d}\epsilon]\epsilon = [T_c/X(T)]\epsilon \tag{7}$$

such deviations imply that $\gamma_{\text{eff}}(\epsilon)$ increases for $\epsilon > \epsilon_{co}$. This behaviour of $\gamma_{\text{eff}}(\epsilon)$ has come to be known as a *characteristic* [13, 14, 21, 22, 24, 27] property of quenched-disordered ferromagnets. Accurate values for the parameters Γ, γ, $a_{\chi 1}^{+}$, $a_{\chi 2}^{+}$, Δ_1 and Δ_2 listed in table 2 are then determined by fitting equations (4) and (5) to the $\gamma_{\text{eff}}(\epsilon)$ and $\Gamma_{\text{eff}}(\epsilon)$ data, depicted in figures 5 and 6 and computed from equations (7) and (3) using the value of T_c deduced by the KF analysis of the $\chi_0(\epsilon)$ data, by means of the non-linear least-squares fitting method. The best theoretical fits to the data so obtained are shown as full curves in figures 5 and 6. In order to verify whether or not the above analysis yields correct values for the parameters

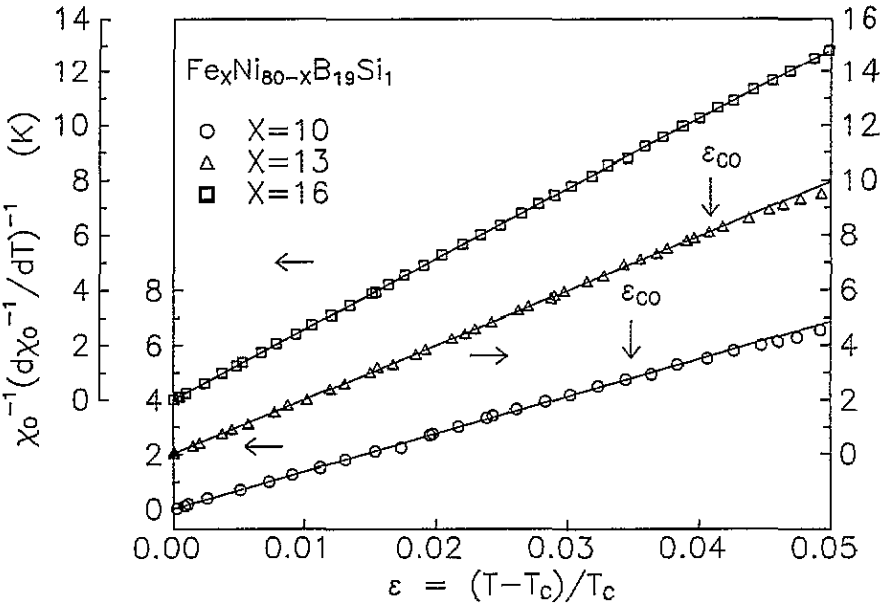

Figure 4. Temperature dependence of the quantity $X(T) \equiv \chi_0^{-1}(\mathrm{d}\chi_0^{-1}/\mathrm{d}T)^{-1}$ in the critical region. Note that only one-quarter of the total number of data points are shown in this figure to maintain clarity and ϵ_{co} denotes the temperature beyond which the data deviate from the least-square fits (full straight lines through the data points) based on equation (6).

of interest, we have constructed the plots of $[\gamma - \gamma_{\mathrm{eff}}(\epsilon)]/\Delta_1\epsilon^{\Delta_1}$ against $\Delta_2\epsilon^{\Delta_2}/\Delta_1\epsilon^{\Delta_1}$ and $\Gamma_{\mathrm{eff}}(\epsilon)$ against N, based on the modified [29] version of equation (4), i.e.

$$[\gamma - \gamma_{\mathrm{eff}}(\epsilon)]/\Delta_1\epsilon^{\Delta_1} = a_{\chi 1}^{+} + a_{\chi 2}^{+}(\Delta_2\epsilon^{\Delta_2}/\Delta_1\epsilon^{\Delta_1}) \tag{8}$$

and equation (5), respectively, with the choice of the parameters given in table 2. Such plots displayed in figures 7 and 8 demonstrate that, consistent with equations (8) and (5), these plots are straight lines with slopes $a_{\chi 2}^{+}$ and Γ, and intercepts on the ordinates $a_{\chi 1}^{+}$ and 0, respectively. In order to bring out clearly the importance of the CTS terms, the deviation plots for the alloys with $x = 10$, 13 and 16 are shown in figure 9. The $\chi_0(\epsilon)$ data, like the $\mathrm{d}\rho(T)/\mathrm{d}T$ data, can be seen to exhibit *systematic* deviations from the KF fits (which totally ignore the CTS terms) throughout the temperature range of the fits, whereas they are evenly scattered around the calculated values in the case of the CTS fits. Moreover, such plots serve as a cross-check for the values of Γ, γ, $a_{\chi 1}^{+}$, $a_{\chi 2}^{+}$, Δ_1 and Δ_2 determined by the above method.

3.3. Bulk magnetization

'Zero-field' quantities like spontaneous magnetization (M_s) and initial susceptibility (χ_0) have been estimated from the magnetization (M) data taken in finite external magnetic fields (H_{ex}) at different temperatures by means of two different extrapolation methods, AA-I and AA-II. In the AA-I method, the 'raw' magnetization data are converted into a set of M^2 versus (H/M) isotherms, which constitute the well known Arrott–Kouvel (AK) plot (figure 10) and upon *parabolic* extrapolation [13, 14, 16, 17] to $(H/M) = 0$ and $M^2 = 0$ yield intercepts on M^2 and H/M axes equal to $M_s^2(T)$ for $T < T_c$ and $\chi_0^{-1}(T)$ for $T > T_c$. By contrast, in

Table 2. Asymptotic and 'correction-to-scaling' critical exponents and critical amplitudes for amorphous $Fe_xNi_{80-x}(B,Si)_{20}$ alloys from the AC susceptibility and bulk magnetization data. Note that the 'so-called' crossover temperature ϵ_{co} is the upper limit of the temperature range used for a given fit.

Alloy composition, Fe/Ni/B/Si	Method	Analysis	Fit range in $10^3\epsilon$	T_c^+ (K)	[γ_{eff}] γ	Δ_1	Δ_2	[Γ_{eff}] $\Gamma = (m_0/h_0)$ (10^{-4} emu g^{-1} Oe^{-1})	$a_{\chi 1}^+$	$a_{\chi 2}^+$	χ^2 (10^{-1})
10/70/19/1	ACS	KF	*0.80–34*	*187.05(5)*	*[1.360(20)]*			[2.90(3)]			
	ACS	CTS	0.80–34	187.05(5)	1.387(12)	0.11(4)	0.55(5)	2.66(14)	0.030(8)	0.32(4)	
	BM	AA-I,KF	0.85–35	186.87(13)	[1.360(30)]			[2.24(6)]			2.23
	BM	AA-I,CTS	0.80–35	*186.88(12)*	*1.385(25)*			*1.92(24)*	*0.037(10)*	*0.32(10)*	*1.25*
	BM	AA-II,KF	0.80–35	187.21(10)	[1.350(30)]			[1.90(10)]			2.00
	BM	AA-II,CTS	0.80–35	187.20(10)	1.385(25)			1.48(22)	0.031(10)	0.32(15)	1.29
13/67/19/1	ACS	KF	0.65–40	268.65(5)	[1.352(18)]			[1.35(4)]			
	ACS	CTS	0.65–40	268.65(5)	1.386(12)	0.11(3)	0.55(4)	1.15(15)	0.035(5)	0.50(5)	
	BM	AA-I,KF	0.62–38	268.50(10)	[1.350(30)]			[1.37(5)]			0.74
	BM	AA-I,CTS	0.62–38	268.47(10)	1.384(26)			1.23(17)	0.030(10)	0.50(10)	0.45
	BM	AA-II,KF	0.62–38	268.75(10)	[1.350(30)]			[1.32(5)]			1.48
	BM	AA-II,CTS	0.62–38	268.75(10)	1.386(24)			1.05(25)	0.032(10)	0.55(10)	0.63
16/64/19/1	ACS	KF	0.40–45	341.51(6)	[1.348(22)]			[0.95(6)]			
	ACS	CTS	0.40–45	341.51(6)	1.386(14)	0.11(3)	0.55(4)	0.75(15)	0.068(7)	0.63(7)	
	BM	AA-I,KF	*0.46–37*	*341.83(12)*	*[1.350(30)]*			[1.26(4)]			5.71
	BM	AA-I,CTS	0.46–37	341.82(13)	1.385(25)			1.03(15)	0.068(15)	0.63(10)	1.08
	BM	AA-II,KF	0.32–37	341.87(13)	[1.348(30)]			[1.07(4)]			2.02
	BM	AA-II,CTS	0.32–37	*341.88(12)*	*1.386(24)*			*0.82(15)*	*0.080(15)*	*0.65(10)*	*1.17*
20/60/20/0	BM	AA-I,KF	0.28–22	425.65(15)	[1.350(30)]			[0.93(7)]			1.46
	BM	AA-I,CTS	0.28–22	425.66(14)	1.384(24)			0.75(15)	0.079(11)	0.55(10)	0.54
	BM	AA-II,KF	0.19–22	425.51(14)	[1.350(30)]			[0.78(8)]			2.14
	BM	AA-II,CTS	0.19–22	425.52(13)	1.387(25)			0.60(15)	0.079(11)	0.59(10)	0.94

Abbreviations: AA, asymptotic analysis (see text); ACS, AC susceptibility; BM, bulk magnetization; CTS, 'correction-to-scaling' analysis; and KF, Kouvel–Fisher analysis.

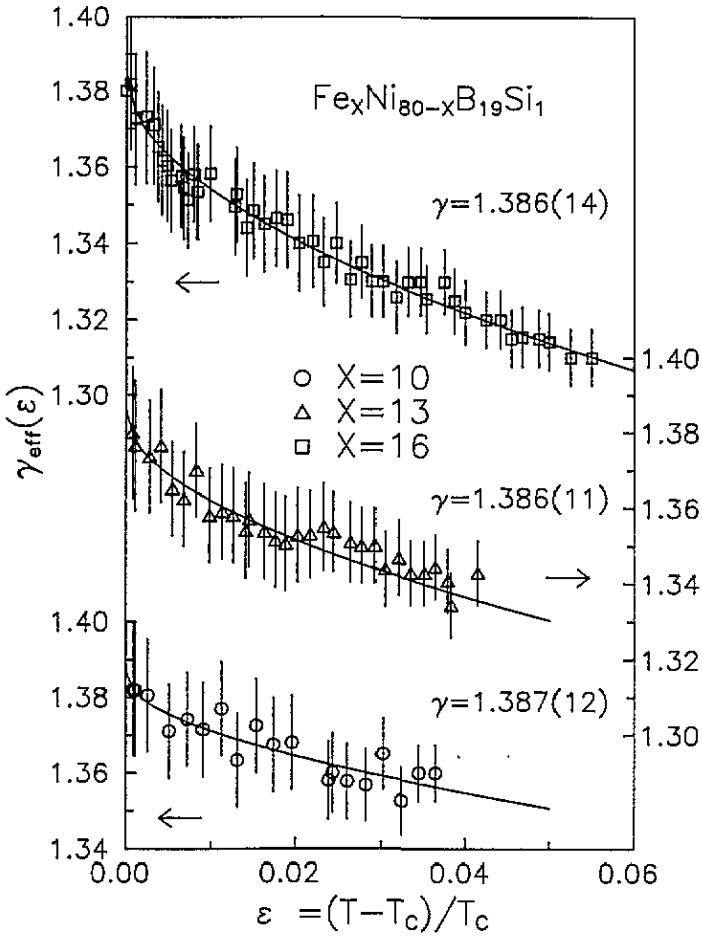

Figure 5. Variation of the *effective* critical exponent for susceptibility, $\gamma_{eff}(\epsilon)$, with reduced temperature in the range $0 \leqslant \epsilon \leqslant 0.06$. Full curves through the data points are the least-squares theoretical fits based on equation (4) while the error limits give the measure of uncertainty in $\gamma_{eff}(\epsilon)$ due to uncertainty in T_c.

the AA-II method, the $M(H = H_{ex} - H_{dem}, T)$ data are used to construct the modified Arrott plot (i.e. $M^{1/\beta}$ versus $(H/M)^{1/\gamma}$ plot shown in figure 11), in which the critical exponents β and γ are varied until $M^{1/\beta}$ versus $(H/M)^{1/\gamma}$ isotherms in a narrow temperature range around T_c are straight and parallel to one another over as wide a range of (H/M) values as possible, and the quantities $M_s(T)$ and $\chi_0^{-1}(T)$ are then computed from the intercepts on the $M^{1/\beta}$ and $(H/M)^{1/\gamma}$ axes obtained by a *linear* extrapolation [13, 14, 19, 22, 24] of the high-field linear portions of the isotherms to $(H/M)^{1/\gamma} = 0$ and $M^{1/\beta} = 0$. Note that the AA-II method gives *more* importance to the high-field data than to the low-field data (i.e. significant deviations from the straight-line behaviour do occur at low fields for isotherms taken at temperatures well below and above T_c, see figure 11) whereas the AA-I method gives *equal* weight to the high- and low-field data. Another important observation [13], which has a direct bearing on the outcome of these extrapolation methods, is that the AK isotherms exhibit increased concave-downward curvature at low fields for $T < T_c$ as the composition $x \to x_c$ so that large gradients near the M^2 axis can introduce large systematic

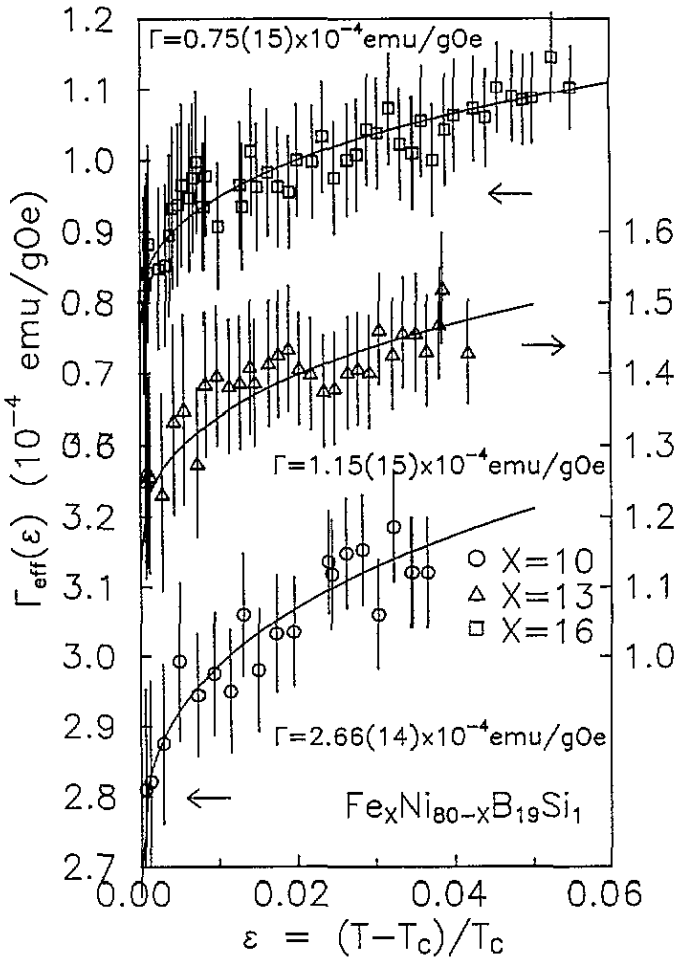

Figure 6. Variation of the *effective* critical amplitude for the susceptibility, $\Gamma_{\text{eff}}(\epsilon)$, with reduced temperature in the range $0 \leqslant \epsilon \leqslant 0.06$. Full curves through the data points are the least-squares theoretical fits based on equation (5) while the error limits give the measure of uncertainty in $\Gamma_{\text{eff}}(\epsilon)$ due to uncertainty in T_c.

errors in the determination of M_s, and hence the values of the exponent β and other fitting parameters derived from such data are less reliable than those extracted from the $M_s(T)$ data obtained by the AA-II method. Figures 12 and 13 compare the corresponding sets of $M_s(T)$ and $\chi_0^{-1}(T)$ data obtained by these extrapolation methods for the investigated alloys in the critical region. In these figures, $M_s(T)$ and $\chi_0^{-1}(T)$ are plotted against the reduced temperature $\epsilon = (T - T_c)/T_c$; the values of T_c used in these plots are displayed in tables 2 and 3 and have been determined by the following method.

Theoretical fits to the $M_s(\epsilon)$ and $\chi_0^{-1}(\epsilon)$ data have been attempted based on the expressions [3–13, 29, 35, 36]

$$M_s(\epsilon) = m_0(-\epsilon)^{\beta}(1 + a_{M1}^{-}(-\epsilon)^{\Delta_1} + a_{M2}^{-}(-\epsilon)^{\Delta_2}) \qquad \epsilon < 0 \tag{9}$$

and

$$M_s(\epsilon) = m_0^{\text{eff}}(-\epsilon)^{\beta_{\text{eff}}} \qquad \epsilon < 0 \tag{10}$$

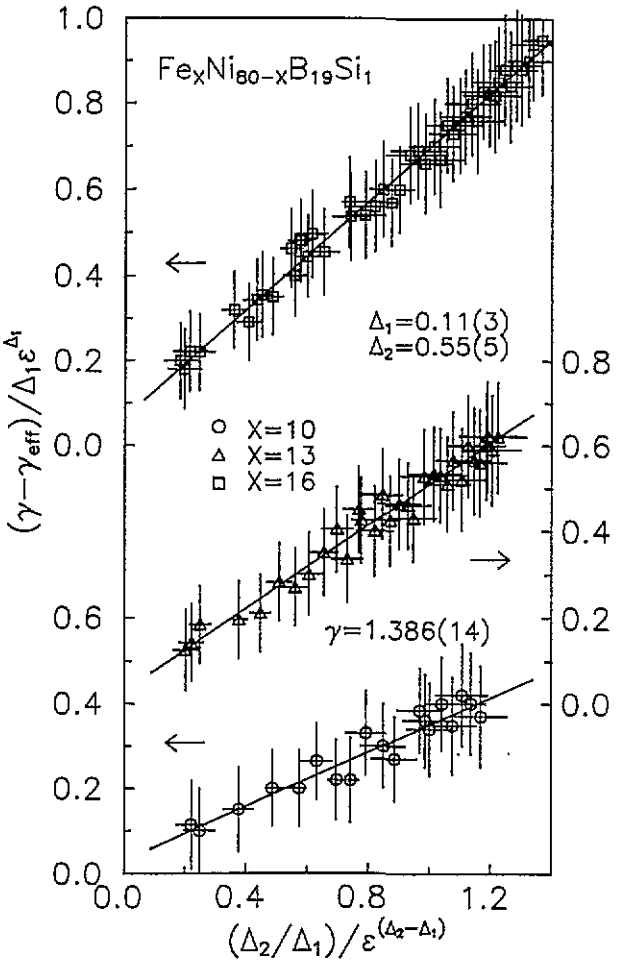

Figure 7. Plots of $[\gamma - \gamma_{\rm eff}(\epsilon)]/\Delta_1\epsilon^{\Delta_1}$ against $(\Delta_2/\Delta_1)\epsilon^{(\Delta_2-\Delta_1)}$ $(= (\Delta_2\epsilon^{\Delta_2}/\Delta_1\epsilon^{\Delta_1}))$ for amorphous $Fe_xNi_{80-x}B_{19}Si_1$ alloys, which make use of the choice of parameters γ, Δ_1 and Δ_2 that gives the best least-squares (LS) fits to the $\gamma_{\rm eff}(\epsilon)$ data based on equation (4). The LS straight-line fits through the data points yield the values for $a^+_{\chi 1}$ (intercept on the ordinate) and $a^+_{\chi 2}$ (slope), which exactly coincide with those obtained through LS fits to the $\gamma_{\rm eff}(\epsilon)$ data directly (i.e. those listed in table 2) based on equation (4) and hence testify to the validity of equation (8).

and the equations (2) and (3) with $\Gamma \equiv (m_0/h_0)$ and $\Gamma_{\rm eff} \equiv (m_0/h_0)_{\rm eff}$, respectively. At first, in analogy with equation (6), equation (10) is cast in the alternative form

$$Y(T) \equiv M_s(T)[{\rm d}M_s(T)/{\rm d}T]^{-1} = (T - T_c)/\beta_{\rm eff} = (T_c/\beta_{\rm eff})\epsilon \qquad (11)$$

and then reasonably accurate values of $\beta_{\rm eff}$ and $\gamma_{\rm eff}$ and T_c are obtained from the slopes and intercepts (on the T axis) of $Y(T)$ versus T and $X(T)$ versus T straight-line plots in the ACR ($|\epsilon| \leqslant |\epsilon_{co}|$). The values for these quantities so deduced are tabulated in tables 2 and 3 and used in equation (10) and (3) to determine $m_0^{\rm eff}$ and $\Gamma_{\rm eff}$ whose values are also included in these tables. The error limits for the *effective* critical amplitudes, critical exponents and T_c have been estimated from the scatter in their values yielded by a detailed 'range-of-fit'

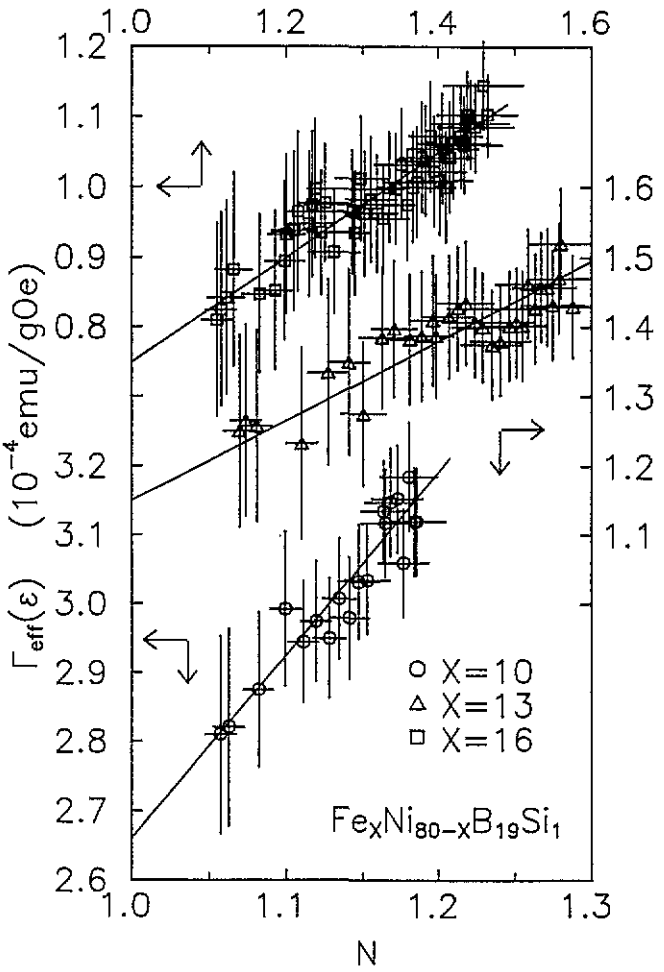

Figure 8. Plots of $\Gamma_{eff}(\epsilon)$ against $N \equiv (1 + a^+_{\chi 1}\epsilon^{\Delta_1} + a^+_{\chi 2}\epsilon^{\Delta_2})\epsilon^{-(a^+_{\chi 1}\Delta_1\epsilon^{\Delta_1} + a^+_{\chi 2}\Delta_2\epsilon^{\Delta_2})}$ for amorphous $Fe_xNi_{80-x}B_{19}Si_1$ alloys, which make use of the choice of parameters Δ_1, Δ_2, $a^+_{\chi 1}$ and $a^+_{\chi 2}$ that gives the best least-squares (LS) fits to the $\gamma_{eff}(\epsilon)$ data based on equation (4). The LS straight-line fits through the data points yield the values for intercept on the ordinate equal to zero and slope equal to Γ and thereby demonstrate the validity of equation (5).

analysis in the ACR. With a view to accommodate data on samples with widely different T_c values in a single figure, the plots of $X(T)$ against ϵ and $Y(T)$ against ϵ are shown in figure 14 instead of the usual $X(T)$ versus T and $Y(T)$ versus T plots. Attempts have also been made to fit (10) and (3) to the $M_s(T)$ and $\chi_0^{-1}(T)$ data taken for $|\epsilon| \leqslant |\epsilon_{co}|$ directly, with the result that the values for the parameters m_0^{eff}, $\Gamma_{eff} = (m_0/h_0)_{eff}$, β_{eff}, γ_{eff} and T_c so determined match very well their corresponding values deduced by the above method (the KF analysis). At this stage, it should be emphasized that the *extrapolated* $M_s(T)$ and $\chi_0^{-1}(T)$ data are bound to have more scatter than the $\chi_{ac}(T)$ data which are *directly* measured because part of the accuracy of the $M(H, T)$ data is lost in the extrapolation (to zero field) process. The scatter in the extrapolated data gives rise to an undesirably large scatter in $\beta_{eff}(\epsilon)$ and $\gamma_{eff}(\epsilon)$ (compare figures 15 and 16 with figure 5), which, in

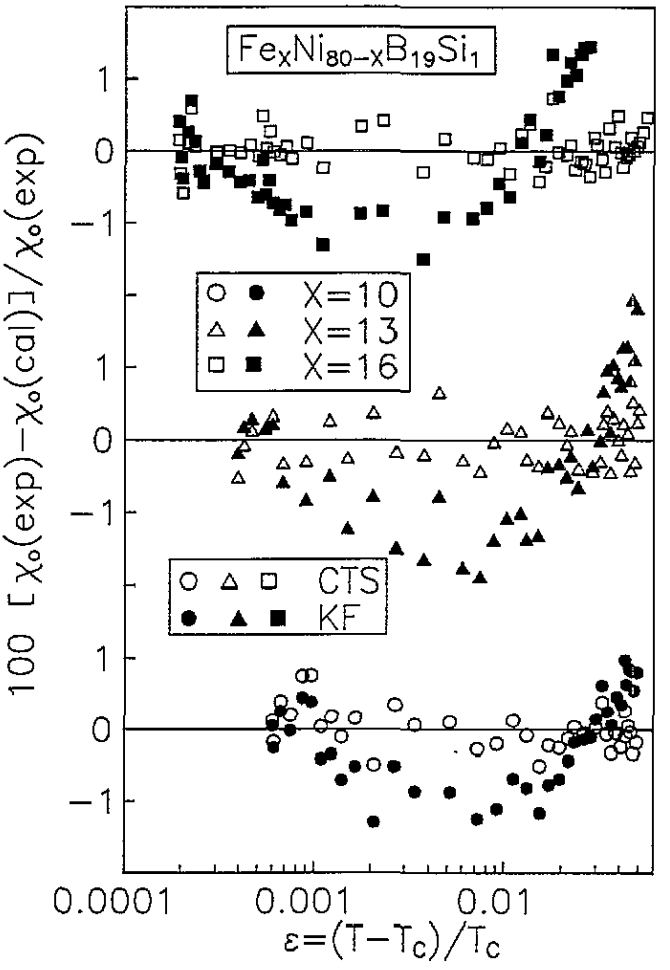

Figure 9. Percentage deviation of the AC susceptibility data, $\chi_0(\epsilon)$, from the best KF (full symbols) and CTS (open symbols) least-squares fits.

turn, precludes the use of the method of analysis, employed earlier to analyse $\chi_{ac}(T)$ data (section 3.2), to extract reliable values for the asymptotic and leading CTS critical amplitudes and critical exponents from such data. We have, therefore, fitted equations (9) and (2) to the $M_s(T)$ and $\chi_0^{-1}(T)$ data taken in the temperature range $|\epsilon| \leqslant |\epsilon_{co}|$ directly using the non-linear least-squares fitting computer program, which varies the fitting parameters m_0 ($\Gamma^{-1} = h_0/m_0$), T_c^- (T_c^+), β (γ) and a_{M1}^- ($a_{\chi 1}^+$) and a_{M2}^- ($a_{\chi 2}^+$) but keeps Δ_1 and Δ_2 constant at their theoretically predicted values, i.e. $\Delta_1 = 0.11$ and $\Delta_2 = 0.55$, to optimize agreement with the experimental $M_s(\epsilon)$ ($\chi_0^{-1}(\epsilon)$) data. The best theoretical fits (shown in figures 12, 13, 15 and 16 by the full curves) with the choice of the parameters given in tables 2 and 3 obtained in this way (henceforth referred to as the CTS analysis) are superior in quality to those (the KF fits) based on equations (10) and (3), as inferred from a substantially reduced value of χ^2 for the former type of fits (tables 2 and 3). Such an improvement in the quality of fits brought about by the inclusion of CTS terms in the theoretical expressions for $M_s(T)$ and $\chi_0^{-1}(T)$, not so apparent from the comparison between theory and experiment

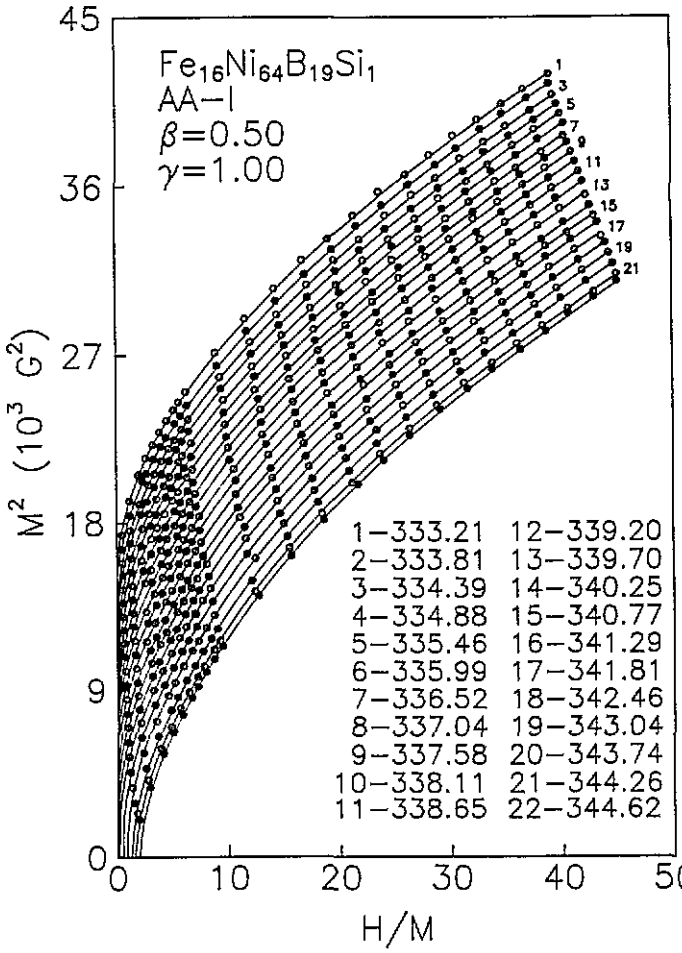

Figure 10. Arrott–Belov–Kouvel (M^2 versus H/M) plot of a-$Fe_{16}Ni_{64}B_{19}Si_1$ at a few representative temperatures around the Curie point.

(depicted in figures 15 and 16) so far as the effective critical exponents $\beta_{\text{eff}}(\epsilon)$ and $\gamma_{\text{eff}}(\epsilon)$ are concerned for reasons already mentioned, is obvious from the deviation plots shown in figure 17 for the data obtained by the AA-II method. Such plots are also *representative* of the nature of deviations observed for the $M_s(T)$ and $\chi_0^{-1}(T)$ data, obtained by the AA-I method, from the KF and CTS fits. The important points that emerge from the analysis presented above (tables 2 and 3) are as follows: (i) The value of T_c does not depend on whether the data analysis includes the CTS terms or not, whereas the same is not true for the asymptotic and effective critical amplitudes and critical exponents. (ii) $M_s(T)$ and $\chi_0^{-1}(T)$ data for a given composition obtained through the same extrapolation method (AA-I or AA-II) yield practically the same value for T_c. (iii) Unlike asymptotic critical exponents and 'correction-to-scaling' amplitudes, Curie temperature and asymptotic critical amplitudes depend on the type of extrapolation used. (iv) The AC susceptibility data and the extrapolated 'zero-field' susceptibility data yield *identical* values (within the uncertainty limits) for all parameters except for Γ and $\Gamma_{\text{eff}}(T_c)$ in the case of the alloy with $x = 10$ ($x = 16$). Note that the value of T_c for the alloy with $x = 16$ deduced from the $M(H, T)$ data is *higher* than that

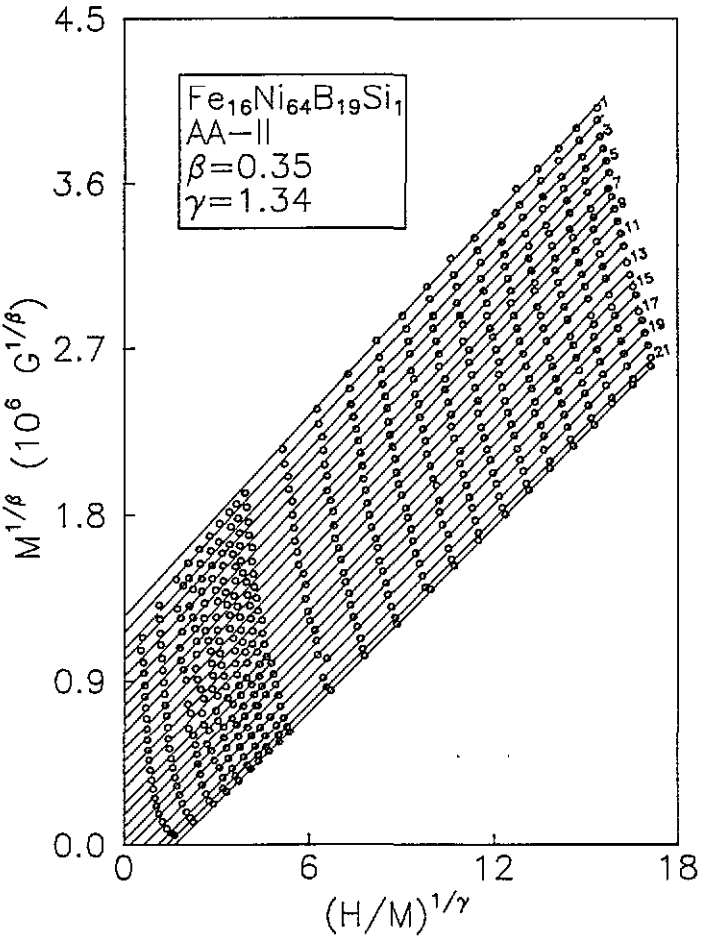

Figure 11. The data shown in figure 8 replotted in the form of $M^{1/\beta}$ versus $(H/M)^{1/\gamma}$ (modified Arrott plot).

determined from the $\chi_{ac}(T)$ data because the $M(H, T)$ measurements were performed after some amount of *structural relaxation* had occurred in the sample when it was heated† to temperatures as high as 400 K during $\chi_{ac}(T)$ measurements.

In order to determine the value of the critical exponent δ, the M versus H isotherms taken at temperatures ranging between the extreme values of T_c yielded by the above-mentioned analysis of the extrapolated $M_s(T)$ and $\chi_0^{-1}(T)$ data, and of $\chi_{ac}(T)$ data, are least-squares-fitted to either of the relations

† The 'kink-point' measurement taken after completing the $\chi_{ac}(T)$ experimental run revealed slight increase in T_c indicating thereby that some amount of stress relief had occurred in this sample. In view of this finding, the $Fe_{20}Ni_{60}B_{20}$ sample was annealed at different temperatures between 400 and 450 K for different durations of time and 'kink-point' (and hence T_c) was monitored after every heat treatment. The electrical resistivity and bulk magnetization measurements were performed on this sample only after ensuring that the subsequent annealing treatment did not increase T_c further. It is, therefore, not surprising that both types ($\rho(T)$ and $M(H, T)$) of measurements yield the same value (within the error limits) of T_c for this sample.

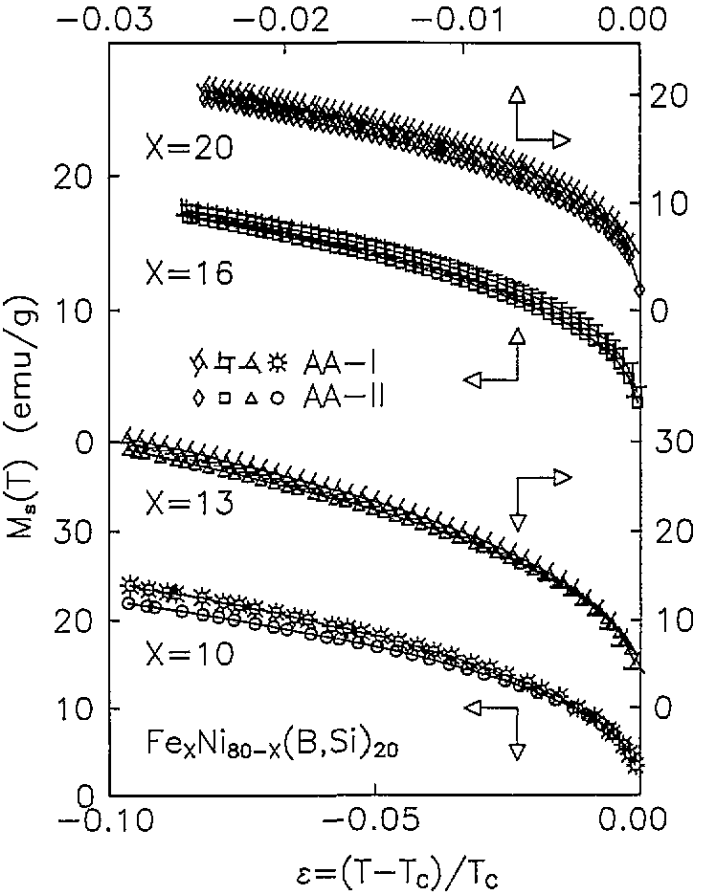

Figure 12. Spontaneous magnetization, M_s, as a function of temperature. For the sake of clarity, only one-quarter of the total number of data points are shown in this figure. The full curves through the data points represent the best least-squares fits to the data based on equation (9).

$$\left.\begin{aligned} M &= A_0 H^{1/\delta} \\ H &= D M^{\delta} \end{aligned}\right\} \qquad \epsilon = 0. \tag{12}$$

It is evident from (12) that a plot of $\ln M$ against $\ln H$ should be a straight line with slope δ^{-1} and intercept on the ordinate equal to $\ln A_0$ for the critical isotherm $M(H, T = T_c)$. Figure 18 depicts such a plot for a-$Fe_{16}Ni_{64}B_{19}Si_1$. A cursory glance at this figure suffices to reveal that only the isotherm taken at $T = T_c$ is indeed a straight line, whereas the isotherms for $T \neq T_c$ exhibit a concave-upward and concave-downward curvature for temperatures just below and above T_c. The curvature in such isotherms becomes more pronounced as the temperature at which a given isotherm is taken deviates more and more from T_c. These features of the $M(H, T)$ data displayed by figure 18 represent a *characteristic* property that the amorphous alloys investigated in this work share with other amorphous ferromagnetic alloys studied earlier [22–24]. Moreover, such plots not only allow determination of the critical exponent δ and critical amplitude A_0 (note that the critical amplitudes D and A_0 in equations (12) are related as $D = A_0^{-\delta}$) from the slope and intercept on the ordinate of the

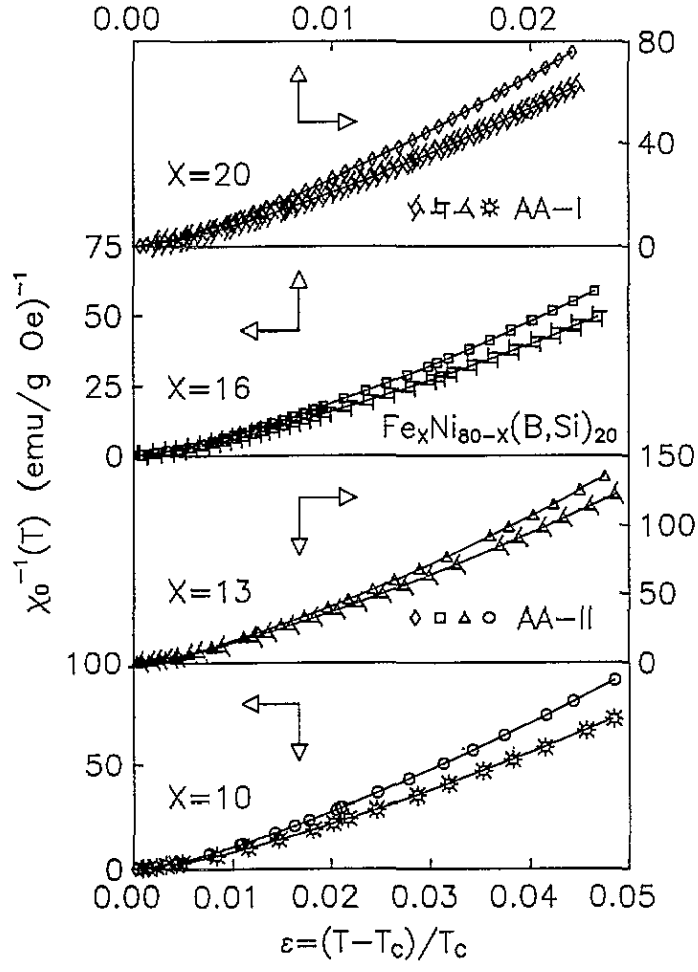

Figure 13. Temperature dependence of the inverse initial susceptibility, χ_0^{-1}, in the critical region for amorphous $Fe_xNi_{80-x}(B,Si)_{20}$ alloys. For the sake of clarity, only one-quarter of the total number of data points are shown in this figure. The full curves through the data points denote the best least-squares fits to the data based on equation (2).

critical isotherm, respectively, but also of the Curie temperature itself. The values of T_c, δ and D determined in this way are listed in tables 4 and 5.

4. Discussion

The experimentally determined values of the asymptotic ($\alpha^{\pm}$, β, γ, δ) and leading 'correction-to-scaling' (Δ_1, Δ_2) critical exponents and of the *universal* ratios involving asymptotic and 'correction-to-scaling' zero-field specific heat and initial susceptibility amplitudes are compared with those predicted by the RG theories [35,37,38,40–44] for pure $d = n = 3$ spin systems with or without isotropic dipolar long-range (IDL) interactions in tables 4–6. With reference to the numerical values for different physical parameters displayed in the tables, the main points that merit attention are the following: (i) The

Table 3. Asymptotic and 'correction-to-scaling' magnetization critical exponents and amplitudes for amorphous $Fe_xNi_{80-x}(B,Si)_{20}$ alloys from bulk magnetization data.

Alloy composition Fe/Ni/B/Si	Method	Analysis	Fit range in $10^3\epsilon$	T_c^- (K)	[β_{eff}] β	[m_0^{eff}] m_0 (emu g^{-1})	a_{M1}^-	a_{M2}^-	χ^2 (10^{-1})
10/70/19/1	BM	AA-I,KF	1.34–87	186.80(14)	[0.416(20)]	[63.4(9)]			1.75
	BM	AA-I,CTS	1.39–85	186.81(14)	0.406(20)	62.0(8)	−0.049(9)	−0.06(2)	0.72
	BM	AA-II,KF	2.22–89	187.29(10)	[0.392(20)]	[53.5(9)]			0.07
	BM	AA-II,CTS	2.16–89	187.28(10)	0.378(15)	52.9(8)	−0.030(15)	0.10(10)	0.05
13/67/19/1	BM	AA-I,KF	0.32–86	268.44(15)	[0.420(20)]	[78.4(9)]			2.80
	BM	AA-I,CTS	0.35–86	268.45(15)	0.400(20)	77.2(5)	−0.037(6)	−0.40(15)	0.93
	BM	AA-II,KF	1.28–87	268.70(10)	[0.405(20)]	[80.0(9)]			1.15
	BM	AA-II,CTS	1.43–87	268.74(10)	0.367(16)	61.7(9)	−0.014(6)	0.57(5)	0.13
16/64/19/1	BM	AA-I,KF	0.20–63	341.89(14)	[0.323(20)]	[57.3(9)]			2.10
	BM	AA-I,CTS	0.23–63	341.91(13)	0.361(16)	74.5(6)	−0.053(10)	−0.70(10)	1.12
	BM	AA-II,KF	0.18–63	341.87(13)	[0.352(20)]	[61.7(9)]			0.75
	BM	AA-II,CTS	0.18–63	341.87(14)	0.360(15)	68.2(7)	−0.059(21)	−0.30(15)	0.58
20/60/20/0	BM	AA-I,KF	0.07–55	425.62(14)	[0.341(20)]	[72.4(9)]			4.00
	BM	AA-I,CTS	0.05–55	425.63(14)	0.363(15)	85.6(6)	−0.031(13)	−0.50(4)	2.17
	BM	AA-II,KF	0.06–55	425.64(14)	[0.379(20)]	[79.4(9)]			1.86
	BM	AA-II,CTS	0.07–55	425.64(13)	0.365(15)	73.0(8)	−0.037(20)	0.40(10)	0.94

Abbreviations: AA, asymptotic analysis (see text); BM, bulk magnetization; CTS, 'correction-to-scaling' analysis; KF, Kouvel–Fisher analysis.

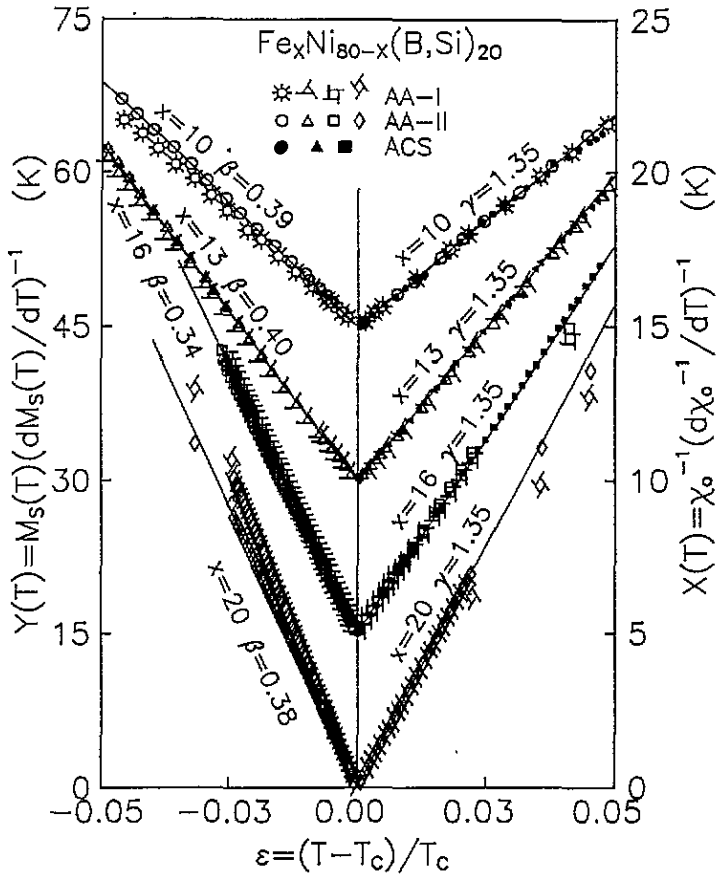

Figure 14. The quantities $X(T)$ and $Y(T)$, deduced from the bulk magnetization (BM) data, as functions of (reduced) temperature, $\epsilon = (T - T)/T_c$, for amorphous $Fe_xNi_{80-x}(B,Si)_{20}$ alloys. In order to highlight the agreement between the BM and AC susceptibility (ACS) data, the values of the quantity $X(T)$ at a few representative temperatures obtained from the ACS data (figure 4) are also included in this figure. For the sake of clarity, only one-quarter (one-eighth) of the total number of data points for $Y(T)$ ($X(T)$) and the KF fits only to the $X(T)$ and $Y(T)$ data, deduced from the $\chi_0^{-1}(T)$ and $M_s(T)$ data, obtained by the AA-II extrapolation method, are shown in this figure.

'zero-field' measurements $\rho(T)$ and $\chi_{ac}(T)$ yield practically the same value for T_c whereas, considering the relatively large uncertainty in the values obtained through the extrapolation methods AA-I and AA-II, this value also conforms well with those deduced using the methods AA-I and AA-II (except for the alloy with $x = 16$ for the reasons already mentioned in the earlier section and in the footnote). (ii) The KF and CTS analyses of the $\chi_{ac}(T)$ and the extrapolated $\chi_0(T)$ data give identical (within the uncertainty limits) results. (iii) The scaling relations $\alpha^+ = \alpha^-$, $\beta + \gamma = \beta\delta$ and $\alpha + \gamma = 2(1 - \beta)$ are obeyed to a high degree of accuracy. (iv) Consistent with $\alpha < 0$, the ratio $(B^+ - A^+/\alpha^+)/(B^- - A^-/\alpha^-) \simeq 1$. (v) The exponents $\alpha^{\pm}$, β, γ, δ, Δ_1 and Δ_2, and the amplitude ratios A^+/A^-, a_{c1}^+/a_{c1}^-, a_{c2}^+/a_{c2}^-, $a_{c1}^+/a_{\chi 1}^+$ and $a_{c2}^+/a_{\chi 2}^+$ *do not* depend on composition. (vi) The ratios a_{c1}^+/a_{c1}^- ($= 0.10 \pm 0.05$) and $a_{c1}^+/a_{\chi 1}^+$ ($= 7 \pm 2$) *characteristic* of ferromagnets with quenched random disorder seem to be *universal* like the corresponding ratios a_{c2}^+/a_{c2}^- and $a_{c2}^+/a_{\chi 2}^+$ in the case of ordered

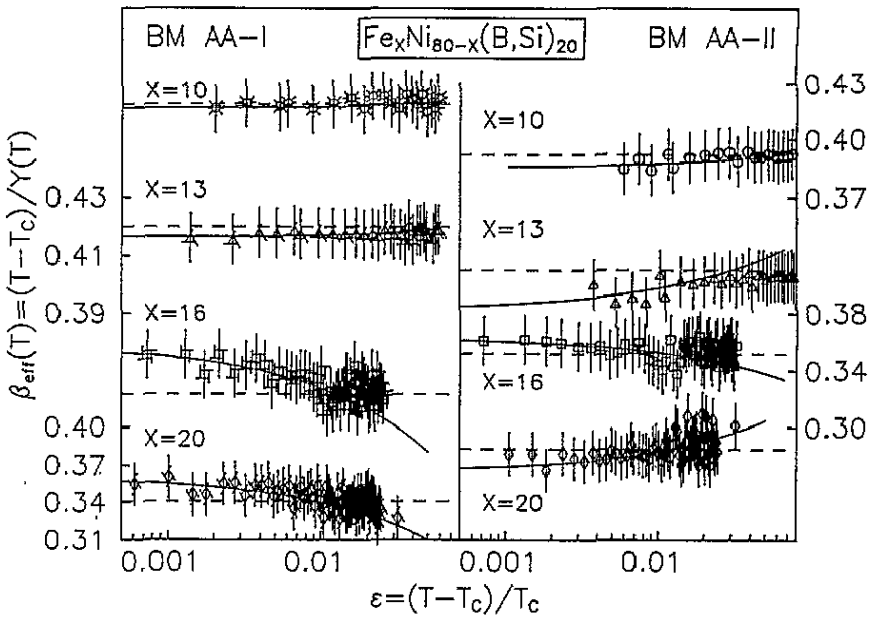

Figure 15. Variation of the *effective* critical exponent for spontaneous magnetization, β_{eff}, with temperature. The full curves and broken straight lines through the data points represent the least-squares fits to the data based on equations (9) and (10), respectively.

spin systems. (vii) The experimental values of α, β, γ, δ, Δ_1, Δ_2, A^+/A^-, a_{c2}^+/a_{c2}^-, $a_{c2}^+/a_{\chi 2}^+$, $m_0/M_s(0)$ and Dm_0^δ/h_0 match very well the RG estimates for the pure $n = d = 3$ spin system with isotropic Heisenberg short-range (ISR) and/or IDL interactions, but the observed values of the ratio $\mu_0 h_0/k_B T_c$ are at least one order of magnitude *lower* than the 3D Heisenberg value. (viii) The theoretical value for the ratio $m_0/M_s(0)$ is in closer agreement with the values yielded by the CTS analysis than with those given by the KF analysis; this finding underscores the need to include the CTS terms in the data analysis. While an excellent agreement between the values of T_c determined from $\rho(T)$ and $\chi_{ac}(T)$ measurements (observation (i) above) refutes the earlier claim [28] that the low-field AC susceptibility is not well suited to study critical behaviour in metallic glasses, the observation (ii) asserts that the deviations from the linear modified Arrott plot isotherms at low fields are of no consequence as far as the asymptotic critical behaviour is concerned (this point will be further substantiated later). Validity of the scaling relations between different critical exponents (exponent equalities) demands that the magnetization data taken in the critical region should satisfy the scaling equation of state (SES)

$$m = f_\pm(h) \tag{13}$$

where plus and minus signs refer to temperatures above and below T_c and $m \equiv M/|\epsilon|^\beta$ and $h \equiv H/|\epsilon|^{\beta+\gamma}$ are the scaled magnetization and scaled fields, respectively. Equation (13) implies that m as a function of h falls on two different universal curves: $f_-(h)$ for $\epsilon < 0$ and $f_+(h)$ for $\epsilon > 0$. Instead of following the customary approach of plotting $\ln m$ against $\ln h$ to ascertain if (13) is obeyed, the magnetization data are tested against an alternative form of SES, i.e.

$$m^2 = \mp a_\pm + b_\pm(h/m) \tag{14}$$

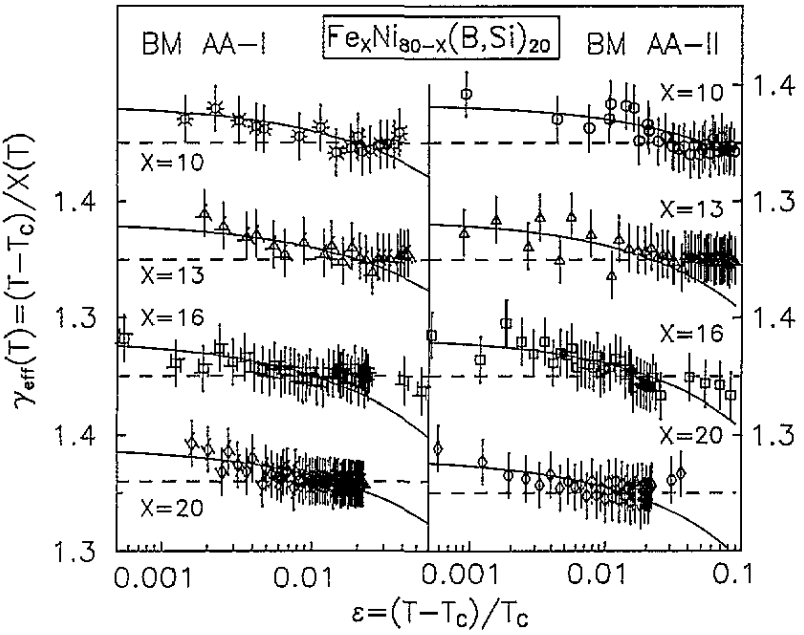

Figure 16. Temperature dependence of the *effective* critical exponent for initial susceptibility, γ_{eff}. The full curves and broken straight lines through the data points represent the least-squares fits to the data based on equations (2) and (3), respectively.

for two main reasons. First, even the slightest deviations of the data from the universal curves $f_-(h)$ and $f_+(h)$, which do not show up clearly in a $\ln m$ versus $\ln h$ plot because of the insensitive nature of the double-logarithmic scale, can be discerned with ease when the same data are plotted in the form of m^2 versus (h/m) plot. Second, the use of the SES form given by (14) permits an independent determination of the critical amplitudes $m_0 = a_-^{1/2}$ and $h_0/m_0 = a_+/b_+$ from the intercepts of the universal curves with m^2 and h/m axes, respectively, in a m^2 versus h/m plot and thereby provides a cross-check for the corresponding values obtained earlier by the KF and/or CTS analysis. A representative m^2 versus h/m plot, which demonstrates the validity of (14) is shown in figure 19. It should be emphasized at this stage that the *sensitivity* of even such a plot does not *suffice* to distinguish clearly between the values of *effective* and true *asymptotic* critical exponents in the present case for the following reason. For temperatures in close proximity to T_c, where a distinction between exponents slightly differing in magnitude should, in principle, be possible, the values of m^2 for a single isotherm span three or more decades, and in order to assess the quality of the data collapse onto the universal curves, the m^2 versus h/m plot has to accommodate a number of such isotherms and hence data values differing by several orders of magnitude at the expense of the sensitivity. However, the values of asymptotic critical amplitudes m_0 and (h_0/m_0) computed from the intercepts of the universal curves so obtained exactly coincide with those listed in tables 2 and 3. Another important point to note is that, in sharp contrast with the low-field behaviour of the modified Arrott plot isotherms (figure 11), no deviations of the data points from the universal curves at low fields are discernible. This finding corroborates our earlier inference that such low-field deviations have no bearing on the critical behaviour. We now consider the physical implications of the considerably lower value of the ratio $\mu_0 h_0/k_B T_c$ for the glassy alloys in question compared

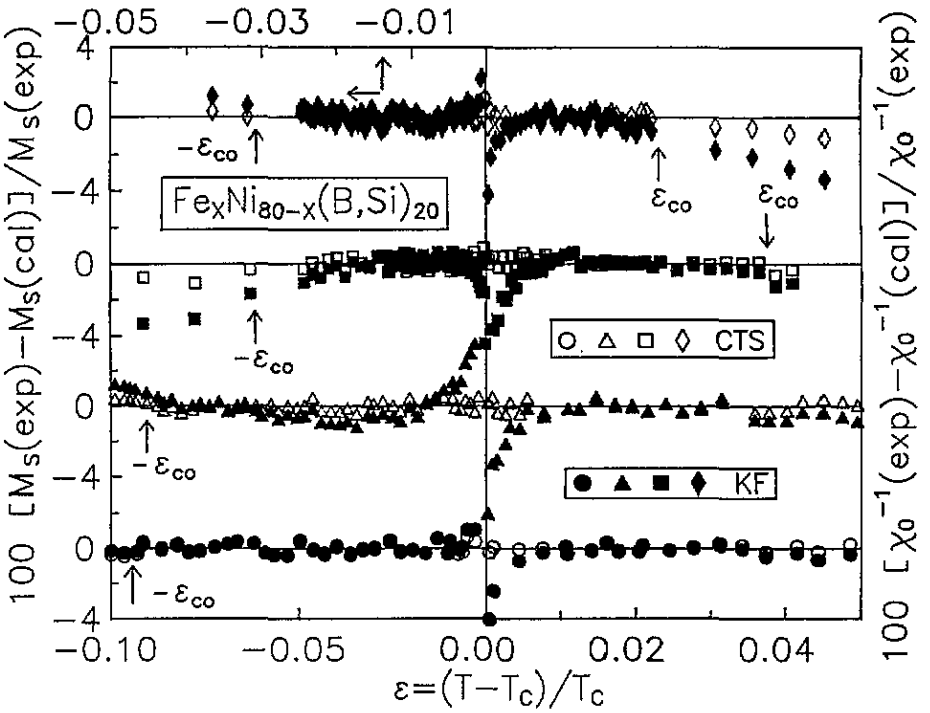

Figure 17. Percentage deviation of the $M_s(\epsilon)$ and $\chi_0^{-1}(\epsilon)$ data, obtained by the AA-II extrapolation method, from the KF (full symbols) and CTS (open symbols) least-squares fits. The arrows indicate the crossover temperature ϵ_{co}.

with that for the isotropic 3D NN Heisenberg ferromagnets (the aforementioned observation (vii)). Since h_0 could presumably be identified with an *effective* exchange interaction field, the product of h_0 and an *average effective* elementary moment (μ_{eff}) involved in the FM–PM phase transition, i.e. the effective exchange energy $\mu_{eff}h_0$, should equal the thermal energy k_BT_c at $T = T_c$. Obviously, this is not true for the investigated amorphous alloys (table 5) unless μ_{eff} has a much higher value than μ_0 (average magnetic moment per alloy atom at 0 K). Considering the fact that the asymptotic and CTS critical exponents as well as all other amplitude ratios possess 3D NN Heisenberg values, the ratio μ_0h_0/k_BT_c is also expected to equal the 3D Heisenberg estimate of 1.58. This is possible only when μ_{eff} takes on the values given in table 5. Moreover, if the concentration of such effective moments is c, then $c = \mu_0/\mu_{eff}$. The values of c so calculated are included in table 5. It is evident from these numerical estimates that only a small fraction of moments (i.e. the Fe spins in the present case because Ni atoms in a-$Fe_xNi_{80-x}B_{19}Si_1$ alloys are known [25] to carry negligibly small moment) actually participates in the FM–PM phase transition and this fraction reduces further as the critical concentration ($x_c^+ \simeq 2.5$ at.% Fe for the alloy series in question [15, 25, 30]) is approached along the FM–PM transition line in the magnetic phase diagram [15] from above. An important consequence of this is that the leading singularity at $T = T_c$ can be detected only in $d\rho_M(T)/dT$ but not in $C_M(T)$ (section 3.1).

The result (observations (v) and (vii) above) that the asymptotic and correction-to-scaling critical exponents as well as the amplitude ratios retain their 'pure' values [35–38, 40, 44] regardless of the alloy composition in the reduced temperature range where, according to the 'unconventional' RG theory [9–12], a crossover to the *new composition-dependent* exponents

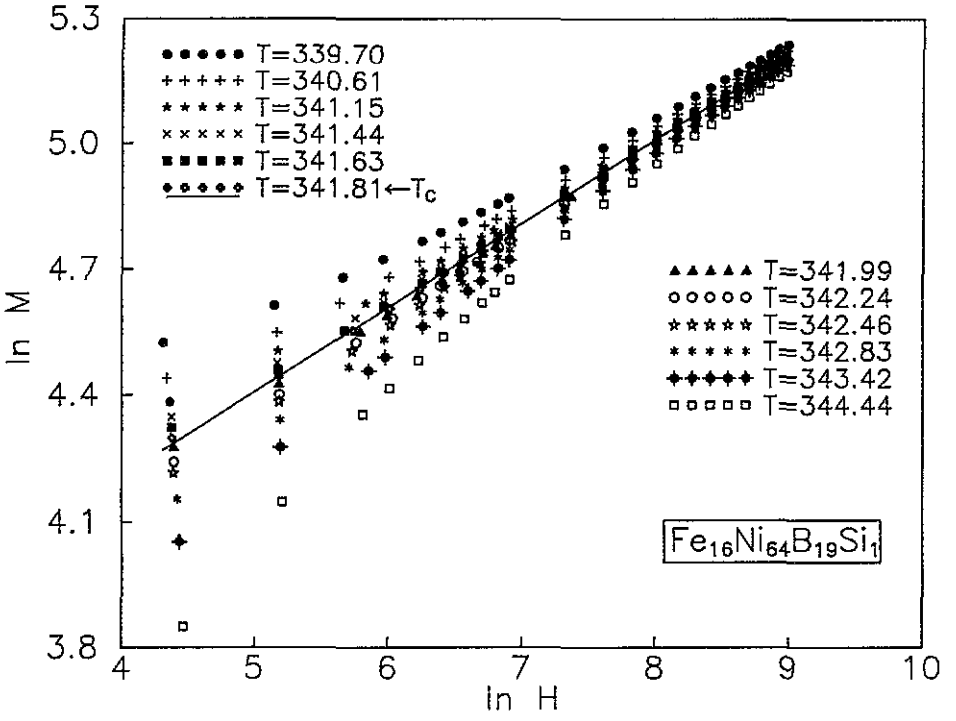

Figure 18. The ln M versus ln H isotherms at a few temperatures around the Curie temperature T_c for a-$Fe_{16}Ni_{64}B_{19}Si_1$. The full straight line through the data represents the best least-squares fit to the critical isotherm (T_c = 341.81 K) based on equation (12) of the text. This plot is representative of the remaining compositions in the investigated alloy series.

should have already taken place testifies to the validity of the theoretical predictions, based on the 'conventional' RG theories, that the critical behaviour of an ordered $n = d = 3$ spin system with $\alpha_p < 0$ remains unaltered in the presence of quenched disorder (and hence to the correctness of the Harris criterion). However, such an agreement between theory and experiment can be put in proper context only when due consideration is given to the following remarks. First, the reliability of the theoretical estimates for some of the quantities quoted in tables 4–6 and obtained through an extrapolation [13] of RG ε-expansion results to $\varepsilon = 4 - d = 1$ is often hard to assess [30]. Thus the role of IDL interactions, if present, can be evaluated better by comparing the experimental values of certain quantities like the exponent α and the ratio A^+/A^- with those determined experimentally for pure $n = d = 3$ spin systems with or without IDL interactions rather than with the theoretical values whose reliability is in doubt. Considering that the antiferromagnet $RbMnF_3$ and ferromagnet EuS are ideal examples of pure ISR exchange and ISR plus IDL exchange $n = d = 3$ spin systems, respectively, the presently determined values of α and A^+/A^- should be compared with the reported [45,46] values $\alpha = -0.10$ and $A^+/A^- = 1.28 \pm 0.02$ for $RbMnF_3$ and $\alpha = -0.124 \pm 0.016$ and $A^+/A^- = 1.54 \pm 0.09$ for EuS. By demonstrating that the values of α determined in this work are the same (within the error limits) as those reported for $RbMnF_3$ and EuS but the A^+/A^- ratio closely conforms only with the value quoted for EuS, this comparison strongly suggests that the IDL interactions are present and affect the asymptotic critical behaviour in the quenched random bond- and site-diluted

Table 4. Asymptotic and 'correction-to-scaling' critical exponents and the scaling relations $\beta + \gamma = \beta\delta$ and $\alpha + \gamma = 2(1 - \beta)$; comparison between theory and experiment. 3D Heisenberg results from [7], [13], [35], [37], [38], [40] and [43].

Alloy composition, Fe/Ni/B/Si	Method/ analysis	T_c (K)	Δ_1	Δ_2	α	β	γ	δ	$\beta+\gamma$	$\beta\delta$	$\alpha+\gamma$	$2(1-\beta)$
10/70/19/1	$d\rho/dT$	187.03(5)	0.11(6)	0.54(10)	−0.114(5)							
	ACS	187.05(5)	0.11(4)	0.55(5)			1.387(12)				1.273(12)	
	ln M vs. ln H	187.01(15)						4.50(5)				
	BM,AA-I,CTS	186.88(12)				0.406(20)	1.385(25)	4.55(5)	1.791(45)	1.85(11)	1.271(30)	1.188(40)
	BM,AA-II,CTS	187.20(10)				0.378(15)	1.385(25)	4.45(5)	1.763(40)	1.68(8)	1.271(30)	1.244(30)
13/67/19/1	$d\rho/dT$	268.64(6)	0.10(5)	0.56(10)	−0.113(5)							
	ACS	268.65(5)	0.11(3)	0.55(4)			1.386(12)				1.273(18)	
	ln M vs. ln H	268.62(15)						4.50(5)				
	BM,AA-I,CTS	268.47(10)				0.400(20)	1.384(26)	4.55(5)	1.784(46)	1.82(11)	1.271(30)	1.200(40)
	BM,AA-II,CTS	268.75(10)				0.367(16)	1.386(24)	4.45(5)	1.753(40)	1.63(8)	1.273(30)	1.266(30)
16/64/19/1	$d\rho/dT$	341.45(5)	0.12(6)	0.55(10)	−0.110(5)							
	ACS	341.51(6)	0.11(3)	0.55(4)			1.386(14)				1.276(4)	
	ln M vs. ln H	341.86(15)						4.86(4)				
	BM,AA-I,CTS	341.82(13)				0.361(16)	1.385(25)	4.90(4)	1.746(41)	1.77(9)	1.275(30)	1.278(32)
	BM,AA-II,CTS	341.88(12)				0.360(15)	1.386(24)	4.86(4)	1.746(39)	1.75(9)	1.276(30)	1.280(30)
20/60/20/0	$d\rho/dT$	425.56(4)	0.11(5)	0.55(8)	−0.114(3)							
	ln M vs. ln H	425.58(15)						4.88(4)				
	BM,AA-I,CTS	425.66(14)				0.363(15)	1.384(24)	4.85(4)	1.747(39)	1.76(8)	1.270(30)	1.274(32)
	BM,AA-II,CTS'	425.52(13)				0.365(15)	1.387(25)	4.90(4)	1.752(40)	1.79(8)	1.273(25)	1.270(30)
3D-Heisenberg			0.115(9) 0.09	0.550(16) 0.48	−0.115(9)	0.365(3)	1.386(4)	4.80(4)	1.751(7)	1.75(3)	1.271(9)	1.270(6)

Abbreviations: AA, asymptotic analysis (see text); ACS, AC susceptibility; BM, bulk magnetization; CTS, 'correction-to-scaling' analysis; ln M vs. ln H, critical isotherm analysis; $d\rho/dT$, temperature derivative of resistivity.

Table 5. Comparison between the experimentally determined and theoretically predicted values for the universal asymptotic amplitude ratios for magnetization. 3D Heisenberg results from [13].

Alloy composition, Fe/Ni/B/Si	Analysis	$M_s(0)$ (emu g^{-1})	$m_0/M_s(0)$	μ_0 (μ_B)	h_0 (kOe)	$\mu_0 h_0/k_B T_c$	μ_{eff} (μ_B)	c (%)	D (10^{-3})	Dm_0^δ/h_0
10/70/19/1	AA-I,KF	42.9(4)	1.48(7)	0.376(4)	284.02(11)	0.038	15.5	2.4		
	AA-I,CTS	42.9(4)	1.44(6)	0.376(4)	322.90(48)	0.044	13.6	2.8	3.387	1 50(40)
	AA-II,KF	42.9(4)	1.25(5)	0.376(4)	281.58(22)	0.038	15.6	2.4		
	AA-II,CTS	42.9(4)	1.24(5)	0.376(4)	357.43(68)	0.048	12.3	3.1	10.713	1.40(38)
13/67/19/1	AA-I,KF	53.9(5)	1.45(4)	0.472(5)	580.71(23)	0.069	10.8	4.3		
	AA-I,CTS	53.9(5)	1.43(3)	0.472(5)	627.64(68)	0.074	10.0	4.6	2.427	1.50(37)
	AA-II,KF	53.9(5)	1.45(6)	0.472(5)	606.06(26)	0.072	10.4	4.5		
	AA-II,CTS	53.9(5)	1.15(3)	0.472(5)	587.6(16)	0.069	10.7	4.4	8.563	1.35(38)
16/64/19/1	AA-I,KF	60.7(5)	1.94(2)	0.528(4)	454.79(23)	0.047	17.7	3.0		
	AA-I,CTS	60.7(5)	1.23(3)	0.528(4)	723.40(86)	0.075	11.1	4.7	0.703	1.45(31)
	AA-II,KF	60.7(5)	0.96(3)	0.528(4)	576.64(45)	0.060	13.9	3.8		
	AA-II,CTS	60.7(5)	1.12(2)	0.528(4)	831.7(13)	0.086	9.67	5.5	1.354	1.33(30)
20/60/20/0	AA-I,KF	71.8(5)	1.01(2)	0.624(5)	778.52(73)	0.077	12.9	4.8		
	AA-I,CTS	71.8(5)	1.19(3)	0.624(5)	1141.3(17)	0.112	8.8	7.1	0.678	1.40(30)
	AA-II,KF	71.8(5)	1.11(2)	0.624(5)	1017.9(12)	0.100	9.8	6.3		
	AA-II,CTS	71.8(5)	1.02(3)	0.624(5)	1216.7(14)	0.119	8.2	7.6	1.217	1.35(30)
3D-Heisenberg			1.37(7)			1.58				1.33(1)

Abbreviations: AA, asymptotic analysis (see text); CTS, 'correction-to-scaling' analysis; KF, Kouvel–Fisher analysis.

Table 6. Comparison between experimentally determined and theoretically predicted values for the specific heat asymptotic critical exponent and amplitude ratios, and for the ratios involving specific heat and susceptibility 'correction-to-scaling' critical amplitudes. 3D Heisenberg results from [13] and [41]–[44].

Alloy composition, Fe/Ni/B/Si	Method/ analysis	α^+/α^-	A^+/A^-	a_{c1}^+/a_{c1}^-	a_{c2}^+/a_{c2}^-	a_{c1}^+/a_{x1}^+	a_{c2}^+/a_{x2}^+
10/70/19/1	$d\rho/dT$	1.00(9)	1.54(3)	0.08(4)	1.04(50)		
	ACS					7.7(20)	4.5(10)
	BM,AA-I,CTS					6.2(30)	4.5(20)
	BM,AA-II,CTS					7.4(30)	4.5(20)
13/67/19/1	$d\rho/dT$	0.98(9)	1.51(3)	0.10(5)	1.00(50)		
	ACS					7.1(25)	4.9(10)
	BM,AA-I,CTS					8.3(50)	4.9(20)
	BM,AA-II,CTS					7.8(45)	4.5(20)
16/64/19/1	$d\rho/dT$	0.99(9)	1.49(3)	0.11(4)	1.03(40)		
	ACS					5.6(15)	4.5(10)
	BM,AA-I,CTS					5.6(25)	4.5(10)
	BM,AA-II,CTS					5.6(20)	4.4(10)
20/60/20/0	$d\rho/dT$	0.99(4)	1.48(3)	0.13(2)	1.02(3)		
	BM,AA-I,CTS					6.7(20)	4.9(10)
	BM,AA-II,CTS					7.0(20)	4.5(10)
3D Heisenberg		1.00	1.51(2)		1.00		4.6(5)

Abbreviations: AA, asymptotic analysis; ACS, AC susceptibility; BM, bulk magnetization; CTS, 'correction-to-scaling' analysis; $d\rho/dT$, temperature derivative of resistivity.

3D Heisenberg spin systems under consideration. Second, the fact that the percolation concentration [15, 25, 30] $p_c \simeq 2.5/80 \simeq 0.031$ for a-$(Fe_pNi_{80-p})B_{19}Si_1$ alloy series lies *well below* the critical concentrations for bond- and site-percolation for nearest-neighbour (NN) exchange interactions on the FCC lattice [47] (which forms an adequate description [16, 26] of the NN atomic configuration in the glassy alloys in question), i.e. $p_c^b = 0.119$ and $p_c^s = 0.195$, respectively, indicates that the exchange interactions in these non-crystalline materials are *not confined* to the *nearest* neighbours only but their range extends far beyond [47] *third* NN distance (r_{3nn}); the range of exchange interactions is, however, too short in comparison with the spin–spin correlation length (at $T \simeq T_c$), which is known [48] to diverge at T_c even for compositions $x \simeq x_c$ in a-(Fe,Ni)–M alloy systems. By contrast, the 'conventional' RG theories are based on quenched random site- and/or bond-diluted *nearest-neighbour* Heisenberg model. Third, since the alloys with $x < x_c$ exhibit spin-glass-like [15] behaviour, long-range RKKY interactions are expected to be present even for samples with composition $x \geqslant x_c$ besides the dominant *direct* Heisenberg isotropic exchange interactions (ILR), which extend well beyond r_{3nn}, and IDL interactions. Based on the present results, one is tempted to conclude that the critical behaviour of $n = d = 3$ spin systems with ILR and IDL interactions is preserved in the presence of RKKY interactions. Though this deduction is consistent with the prediction of a recent theory [49], which treats RKKY interactions within the framework of the spherical model for a ferromagnet with simple cubic lattice, rigorous theoretical calculations, which deal with a 3D Heisenberg spin system in which spins are interacting with one another via long-range isotropic exchange (range far

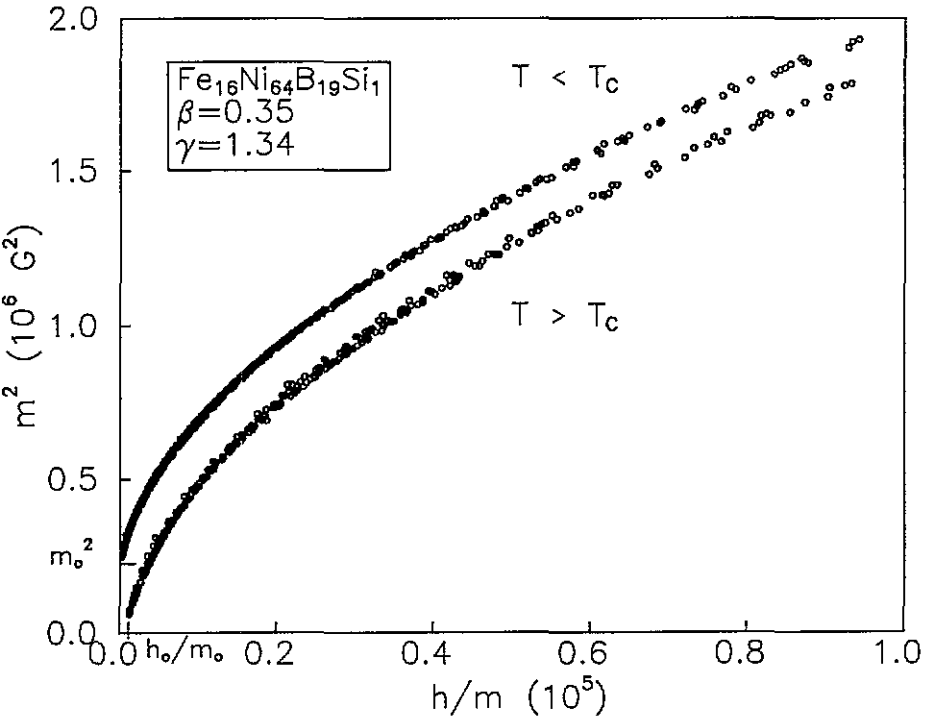

Figure 19. The m^2 versus h/m scaling plot for a-$Fe_{16}Ni_{64}B_{19}Si_1$. Similar scaling plots are obtained for other compositions.

exceeding r_{3nn}), IDL and RKKY interactions, are called for, on the theoretical front, whereas the experimental results of the type presented in this paper on compositions very close to x_c are needed, on the experimental side, to pinpoint the role of RKKY interactions since they are comparable in strength to the direct isotropic Heisenberg interactions for $x \simeq x_c$. Experimental investigations of the asymptotic critical behaviour in alloys with composition just above x_c are planned in future.

5. Conclusions

The results of the present investigation permit us to draw the following conclusions:

In conformity with the Harris criterion and the predictions of the 'conventional' RG theories, asymptotic critical behaviour of quenched random-exchange Heisenberg ferromagnets is the same as that of the pure (ordered) $n = d = 3$ spin system with $\alpha_p < 0$. This conclusion is based on the observation that the asymptotic and 'correction-to-scaling' critical exponents and the corresponding amplitude ratios remain unaltered from their pure values as the critical concentration is approached along the FM–PM phase transition line of the magnetic phase diagram.

The effect of the IDL interactions of the type $[(g_s\mu_B)^2/r^d][d(r_\mu r_\nu/r^2) - \delta_{\mu\nu}]S_0^\mu S_r^\nu$, where g_s is the splitting factor and d is the space dimensionality, on the asymptotic critical behaviour is mainly felt through the *enhanced* value of the A^+/A^- ratio as these interactions

leave other universal amplitude ratios and critical exponents practically unaltered from their values in the ISR case.

Only a small fraction of spins (moments) actually participates in the FM–PM transition for compositions not too far above the critical concentration and this fraction reduces further at a very rapid rate as $x \to x_c$. This result is of paramount importance as far as the understanding of re-entrant behaviour at low temperatures in ferromagnets with composition just above x_c is concerned.

The amplitude ratios a_{c1}^{+}/a_{c1}^{-} and $a_{c1}^{\pm}/a_{\chi 1}^{+}$, *characteristic* of ferromagnets with quenched random disorder, are *universal* in the same sense as the ratios a_{c2}^{+}/a_{c2}^{-} and $a_{c2}^{+}/a_{\chi 2}^{+}$ are for ordered (crystalline) ferromagnets. No theoretical estimates are presently available for the former set of ratios. It is hoped that the present results will motivate theorists to undertake calculation of these ratios and thereby significantly contribute to the understanding of asymptotic critical behaviour of quenched random-exchange Heisenberg ferromagnets.

Since *crossover* to a random fixed point, characterized by a set of *new* critical exponents whose values substantially differ from the 3D Heisenberg ones, has not been observed even for temperatures as close to T_c as $\epsilon \simeq 10^{-4}$, long-range *anisotropic dipolar* interactions and *isotropic* long-range *exchange* interactions of the form $-(J_{\infty} r^{d+\sigma}) S_0 \cdot S_r$, where $0 < \sigma < 2$ and $\sigma < (2 - \eta)$, which render ISR Heisenberg fixed point unstable, are both *absent* in the glassy alloys in question.

That the universality hypothesis, which asserts that the range and type of interaction both are of no consequence as long as the spin–spin correlation length diverges at T_c, is basically correct is vindicated by the result that the ISR Heisenberg-like critical behaviour is retained despite the presence of long-range *direct* exchange interactions (range far exceeding r_{3nn} but too short compared to the spin–spin correlation length).

Acknowledgments

This work was supported by the Department of Science and Technology, New Delhi, through Grant No SP/S2/M21/86. One of us (MSR) would like to thank the Department of Atomic Energy, India, for financial assistance.

References

[1] Rushbrooke G S, Muse R A, Stephenson R L and Pirnie K 1972 *J. Phys. C: Solid State Phys.* **5** 3371
[2] Brown E, Essam J W and Place C M 1975 *J. Phys. C: Solid State Phys.* **8** 321
[3] Lubensky T C 1975 *Phys. Rev.* B **11** 3573
[4] Khmel'nitzki D E 1976 *Sov. Phys.–JETP* **41** 981 (1975 *Zh. Eksp. Teor. Fiz.* **68** 1960)
[5] Grinstein G and Luther A 1976 *Phys. Rev.* B **13** 1329
[6] Weinrib A and Halperin B I 1983 *Phys. Rev.* B **27** 413
[7] Jug G 1983 *Phys. Rev.* B **27** 609
[8] Harris A B 1974 *J. Phys. C: Solid State Phys.* **7** 1671
[9] Sobotta G and Wagner D 1980 *J. Magn. Magn. Mater.* **15–18** 257
[10] Sobotta G and Wagner D 1985 *J. Magn. Magn. Mater.* **49** 77 and references therein
[11] Cordeiro C E and Wagner D 1988 *Phys. Rev.* B **38** 8974
[12] Heuer H O and Wagner D 1988 *J. Physique Coll.* **49** C8 1265; 1989 *Phys. Rev.* B **40** 2502
[13] Kaul S N 1985 *J. Magn. Magn. Mater.* **53** 5 and references therein
[14] Kaul S N 1984 *IEEE Trans. Magn.* **MAG-20** 1290
[15] Kaul S N 1993 *Proc. Int. Conf. on Disordered Materials (Indore, India, 1991)* ed S K Srivastava (Allahabad: INDIAS) p 196
[16] Kaul S N 1980 *Phys. Rev.* B **22** 278; 1981 *Phys. Rev.* B **23** 1205; 1981 *Phys. Rev.* B **24** 6550

[17] Kaul S N and Rosenberg M 1981 *Phil. Mag.* **44** 357; 1982 *Solid State Commun.* **41** 857
[18] Olivier M, Ström-Olsen J O, Altounin Z and Williams G 1983 *J. Appl. Phys.* **53** 7696
[19] Manheimer M A, Bhagat S M and Chen H S 1983 *J. Magn. Magn. Mater.* **38** 147
[20] Böhnke G, Kaul S N, Kettler W and Rosenberg M 1983 *Solid State Commun.* **48** 743
[21] Marohnic Z and Babic E 1985 *Rapidly Quenched Metals* ed S Steeb and H Warlimont (Amsterdam: Elsevier) p 1063
Drobac D and Marohnic Z 1985 *Rapidly Quenched Metals* ed S Steeb and H Warlimont (Amsterdam: Elsevier) p 1133
[22] Kaul S N, Kellner W U and Kronmüller H 1987 *Key Eng. Mater.* **13–15** 669
Kellner W U, Fähnle M, Kronmüller H and Kaul S N 1987 *Phys. Status Solidi* b **144** 397
[23] Hargraves P and Dunlap R A 1988 *J. Phys. F: Met. Phys.* **18** 553; 1988 *J. Magn. Magn. Mater.* **75** 378
[24] Reisser R, Fähnle M and Kronmüller H 1991 *J. Magn. Magn. Mater.* **97** 83
[25] Kaul S N 1981 *IEEE Trans. Magn.* **MAG-17** 1208
[26] Kaul S N 1983 *Phys. Rev.* B **27** 5761
[27] Zadro K, Babic E and Miljak M 1984 *J. Magn. Magn. Mater.* **43** 261
[28] Güntzel U and Westerholt K 1990 *Phys. Rev.* B **41** 740
[29] Kaul S N 1988 *Phys. Rev.* B **38** 9178
[30] Kaul S N and Sambasiva Rao M 1991 *Phys. Rev.* B **43** 11 240
[31] Kaul S N and Methfessel S 1983 *Solid State Commun.* **47** 147
[32] Fisher M E and Langer J S 1968 *Phys. Rev. Lett.* **20** 665
[33] Craven R A, Tsuei C C and Stephens R 1978 *Phys. Rev.* B **17** 2206
[34] Babic E, Marohnic Z, Saub K, Fogarassy B and Kemeny T 1980 *J. Magn. Magn. Mater.* **15–18** 249
[35] Aharony A 1976 *Phase Transitions and Critical Phenomena* vol 6, ed C Domb and M S Green (New York: Academic) p 357
[36] Kaul S N 1994 *Phase Transitions* **47** 23
[37] LeGuillou J C and Zinn-Justin J 1980 *Phys. Rev.* B **21** 3976
[38] Gorishny S G, Larin S A and Tkachov F V 1984 *Phys. Lett.* **101A** 120
[39] Kouvel J S and Fisher M E 1964 *Phys. Rev.* A **136** 1626
[40] Brezin E, LeGuillou J C and Zinn-Justin J 1974 *Phys. Lett.* **47A** 285
[41] Aharony A and Hohenberg P C 1976 *Phys. Rev.* B **13** 3081
[42] Aharony A and Ahlers G 1980 *Phys. Rev. Lett.* **44** 782
[43] Bagnuls C and Bervillier C 1985 *Phys. Rev.* B **32** 7209
[44] Bervillier C 1986 *Phys. Rev.* B **34** 8141
[45] Ahlers G and Kronblit A 1975 *Phys. Rev.* B **12** 1938
[46] Kornblit A, Ahlers G and Buehler E 1978 *Phys. Rev.* B **17** 282
[47] Stinchcombe R B 1983 *Phase Transitions and Critical Phenomena* vol 7, ed C Domb and M S Green (New York: Academic) p 151
[48] Tarvin J A, Shirane G, Birgeneau R J and Chen H S 1978 *Phys. Rev.* B **17** 241
Salamon M B and Murani A P 1984 *J. Appl. Phys.* **55** 1688
[49] Beutler R and Fähnle M 1989 *Phys. Rev.* B **40** 11 417